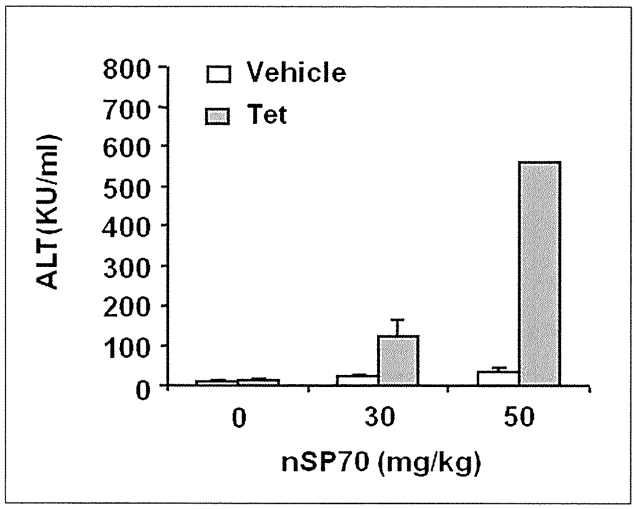

(A)

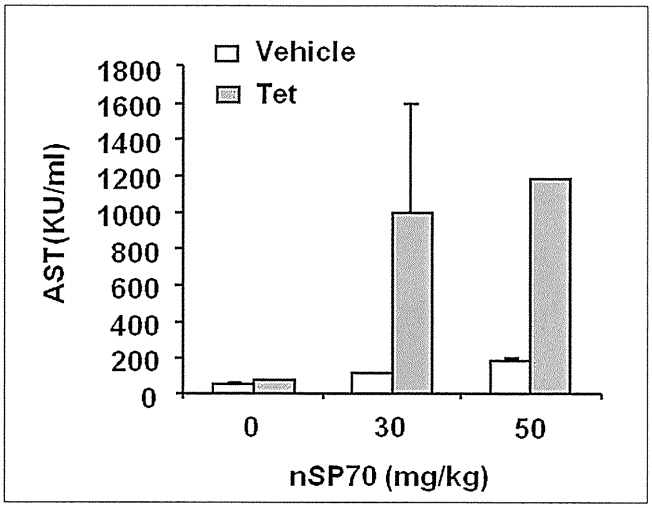

(B)

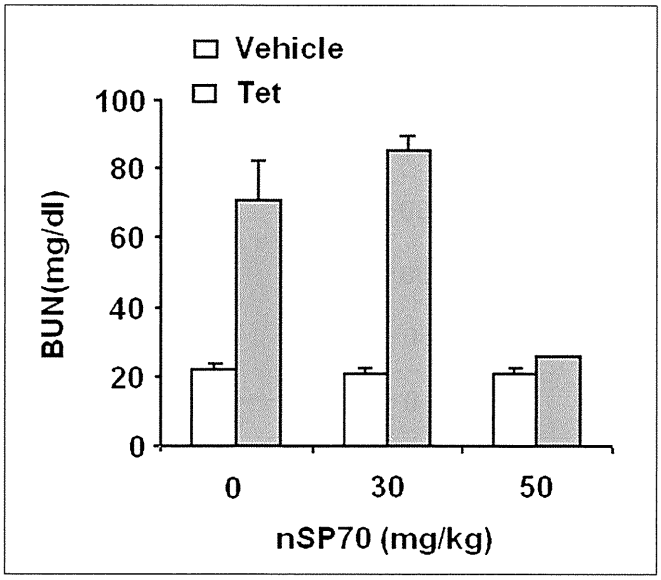

(C)

Fig. 2: Effect of nSP70 on tetracycline (Tet)-induced toxicity Mice were injected intraperitoneally with Tet at 0 (open column) or 100 mg/kg (gray column) and intravenously with nSP70 at the indicated doses. After 24 h, the serum was collected. Shown are the levels of ALT (A), AST (B), and BUN (C). One of 4 mice died when co-treated with nSP70 (30 mg/kg) and Tet (100 mg/kg), and 2 of 4 mice died when co-treated with nSP70 (50 mg/kg) and Tet (100 mg/kg). Data are means or means ± SEM (n = 2–4)

was also reported in mice co-treated with nSP70 and cisplatin (Nishimori et al. 2009a). However, the mechanism by which these decrease the BUN level remains to be determined.

In conclusion, we found that nSP70 cause synergistic toxicity when combined with some clinically used drugs, although the synergistic effects differ between chemicals. One combination was lethal, and the others resulted in tissue injury. These studies suggest that evaluation of possible synergistic adverse effects with pharmaceutical drugs may be important for assessing the safety of nano-sized particles.

4. Experimental

4.1. Materials

The nSP70 nanoparticles were obtained from Micromod Partikeltechnologie GmnH (Rostock, Germany). The mean diameter of the particles, as analyzed by a Zetasizer (Sysmex Co., Kobe, Japan), was 55.7 nm, and the particles were spherical and nonporous. The particles were stored at 25 mg/ml as an aqueous suspension. The suspensions were thoroughly dispersed by sonication before use and diluted in water. An equal volume of solution was injected for each treatment. Acetaminophen, tetracycline, and trazodone were dissolved in saline solution, and 5-aminosalicylic acid was suspended in 1% sodium salt of carboxy methyl cellulose. All reagents were of research grade.

4.2. Animals

Eight-week-old BALB/c male mice were purchased from Shimizu Laboratory Supplies Co., Ltd. (Kyoto, Japan). Mice were maintained in controlled environment (23 ± 1.5 °C; 12-h light/12-h dark cycle) with free access to standard rodent chow and water. The mice were given 1 week to adapt before experiments. All of the experimental protocols complied with the ethical guidelines of the Graduate School of Pharmaceutical Sciences, Osaka University.

4.3. Biochemical analysis

Serum alanine aminotransferase (ALT), aspartate aminotransferase (AST), and blood urea nitrogen (BUN) were measured using commercially available kits according to the manufacturer's protocols (WAKO Pure Chemical, Osaka, Japan).

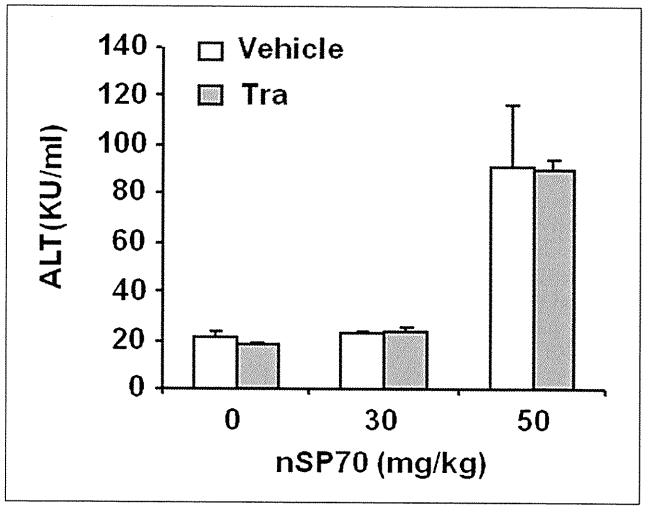

(A)

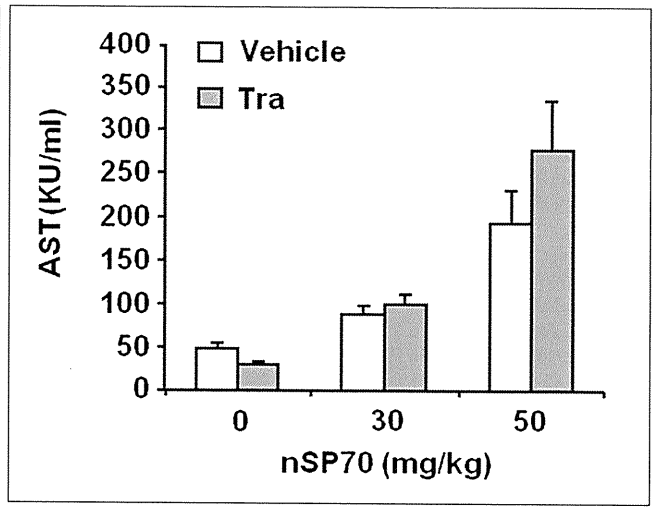

(B)

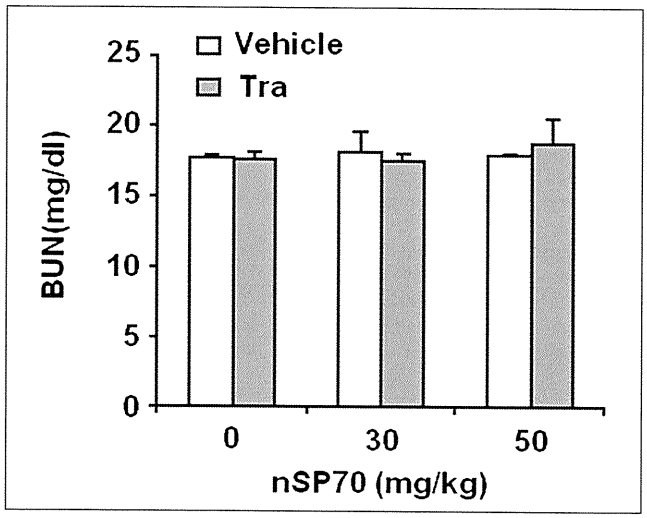

(C)

Fig. 3: Effect of nSP70 on trazodone (Tra)-induced toxicity Mice were injected intraperitoneally with Tra at 0 (open column) or 100 mg/kg (gray column) and intravenously with nSP70 at 30 or 50 mg/kg. After 24 h, the serum was collected. Shown are the levels of ALT (A), AST (B), and BUN (C). Data are means ± SEM (n = 4)

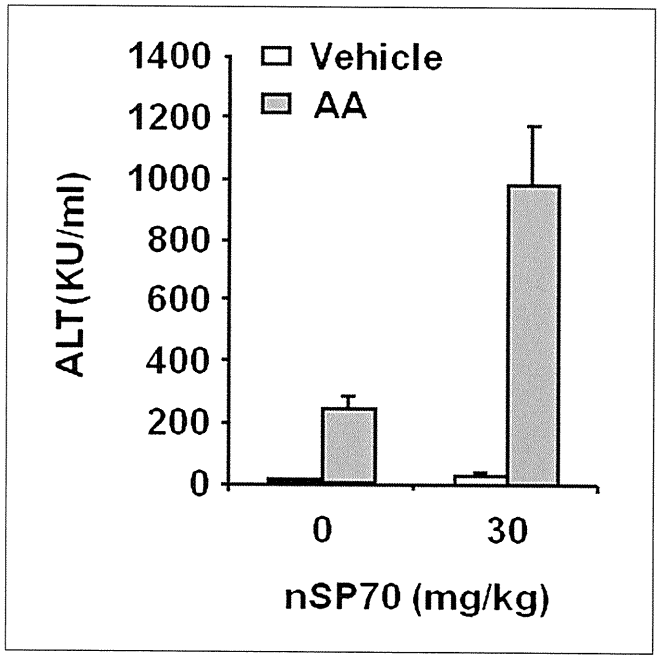

(A)

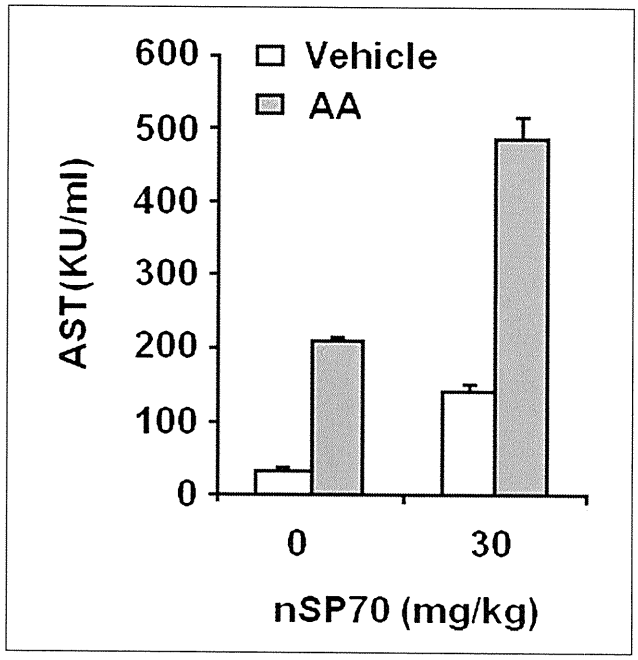

(B)

Fig. 4: Effect of nSP70 on acetaminophen (AA)-induced toxicity Mice were injected intraperitoneally with AA at 0 (open column) or 500 mg/kg (gray column) and intravenously with nSP70 (30 mg/kg). After 24 h, the serum was collected. Shown are the levels of ALT (A) and AST (B). Data are means ± SEM (n = 4)

Acknowledgements: The authors thank all members of our laboratory for their useful comments and discussion. This study was supported by a grant from the Ministry of Health, Labor, and Welfare of Japan.

References

Ali MM, Frei E, Straub J, Breuer A Wiessler M (2002) Induction of metallothionein by zinc protects from daunorubicin toxicity in rats. Toxicology 179: 85–93.

Byrne JD Baugh JA (2008) The significance of nanoparticles in particle-induced pulmonary fibrosis. Mcgill J Med 11: 43–50.

Chun LJ, Tong MJ, Busuttil RW Hiatt JR (2009) Acetaminophen hepatotoxicity and acute liver failure. J Clin Gastroenterol 43: 342–349.

Deltenre P, Berson A, Marcellin P, Degott C, Biour M Pessayre D (1999) Mesalazine (5-aminosalicylic acid) induced chronic hepatitis. Gut 44: 886–888.

Dutta D, Sundaram SK, Teeguarden JG, Riley BJ, Fifield LS, Jacobs JM, Addleman SR, Kaysen GA, Moudgil BM Weber TJ (2007) Adsorbed proteins influence the biological activity and molecular targeting of nanomaterials. Toxicol Sci 100: 303–315.

Grisham MB, Ware K, Marshall S, Yamada T Sandhu IS (1992) Prooxidant properties of 5-aminosalicylic acid. Possible mechanism for its adverse side effects. Dig Dis Sci 37: 1383–1389.

Herzog R Leuschner J (1995) Experimental studies on the pharmacokinetics and toxicity of 5-aminosalicylic acid-O-sulfate following local and systemic application. Arzneimittelforschung 45: 300–303.

Jansen RW, Molema G, Harms G, Kruijt JK, van Berkel TJ, Hardonk MJ Meijer DK (1991) Formaldehyde treated albumin contains monomeric and polymeric forms that are differently cleared by endothelial and Kupffer cells of the liver: evidence for scavenger receptor heterogeneity. Biochem Biophys Res Commun 180: 23–32.

Jin CY, Zhu BS, Wang XF Lu QH (2008) Cytotoxicity of titanium dioxide nanoparticles in mouse fibroblast cells. Chem Res Toxicol 21: 1871–1877.

Kamps JA, Morselt HW, Swart PJ, Meijer DK Scherphof GL (1997) Massive targeting of liposomes, surface-modified with anionized albumins, to hepatic endothelial cells. Proc Natl Acad Sci U S A 94: 11681–11685.

Kovacic P (2005) Role of oxidative metabolites of cocaine in toxicity and addiction: oxidative stress and electron transfer. Med Hypotheses 64: 350–356.

Kunin CM (1971) Hepatorenal toxicity of tetracycline. Minn Med 5: 532–533.

Margetts PJ, Churchill DN Alexopoulou I (2001) Interstitial nephritis in patients with inflammatory bowel disease treated with mesalamine. J Clin Gastroenterol 32: 176–178.

Nishimori H, Kondoh M, Isoda K, Tsunoda S, Tsutsumi Y Yagi K (2009a) Influence of 70 nm silica particles in mice with cisplatin or paraquat-induced toxicity. Pharmazie 64 : 395–397.

Nishimori H, Kondoh M, Isoda K, Tsunoda S, Tsutsumi Y Yagi K (2009b) Silica nanoparticles as hepatotoxicants. Eur J Pharm Biopharm 72: 496–501.

Popov PG, Vaptzarova KI, Kossekova GP Nikolov TK (1972) Fluorometric study of tetracycline-bovine serum albumin interaction. The tetracyclines-a new class of fluorescent probes. Biochem Pharmacol 21: 2363–2372.

Powis G (1974) A study of the interaction of tetracycline with human serum lipoproteins and albumin. J Pharm Pharmacol 26: 113–118.

Sharma CS, Sarkar S, Periyakaruppan A, Barr J, Wise K, Thomas R, Wilson BL Ramesh GT (2007) Single-walled carbon nanotubes induces oxidative stress in rat lung epithelial cells. J Nanosci Nanotechnol 7: 2466–2472.

Xie G, Sun J, Zhong G, Shi L Zhang D (2009) Biodistribution and toxicity of intravenously administered silica nanoparticles in mice. Arch Toxicol, in press.

Xu JJ, Henstock PV, Dunn MC, Smith AR, Chabot JR de Graaf D (2008) Cellular imaging predictions of clinical drug-induced liver injury. Toxicol Sci 105: 97–105.

Yang ST, Wang X, Jia G, Gu Y, Wang T, Nie H, Ge C, Wang H Liu Y (2008) Long-term accumulation and low toxicity of single-walled carbon nanotubes in intravenously exposed mice. Toxicol Lett 181: 182–189.

Ye Y, Liu J, Xu J, Sun L, Chen M Lan M (2010) Nano-SiO2 induces apoptosis via activation of p53 and Bax mediated by oxidative stress in human hepatic cell line. Toxicol *In Vitro* 24: 751–758.

ELSEVIER

Pathological changes in tight junctions and potential applications into therapies

Azusa Takahashi, Masuo Kondoh, Hidehiko Suzuki, Akihiro Watari and Kiyohito Yagi

Laboratory of Bio-Functional Molecular Chemistry, Graduate School of Pharmaceutical Sciences, Osaka University, Osaka 565-0871, Japan

Epithelial cells are pivotal in the separation of the body from the outside environment. Orally administered drugs must pass across epithelial cell sheets, and most pathological organisms invade the body through epithelial cells. Tight junctions (TJs) are sealing complexes between adjacent epithelial cells. Modulation of TJ components is a potent strategy for increasing absorption. Inflammation often causes disruption of the TJ barrier. Molecular imaging technology has enabled elucidation of the dynamics of TJs. Molecular pathological analysis has shown the relationship between TJ components and molecular pathological conditions. In this article, we discuss TJ-targeted drug development over the past 2 years.

During evolution from single-celled to multi-celled organisms, a compartment system developed to separate the inside of the body from the outside environment. This compartment system is made up of epithelial and endothelial cell sheets. Sealing of the intercellular space between individual epithelial or endothelial cells is crucial for compartmentalization.

Tight junctions (TJs) are the apical-most component of intercellular seals. TJs are directly involved both in the sealing of paracellular spaces and in two major functions of membranes: the barrier function and the fence function [1,2]. The barrier function is the first line of defense against pathogenic microorganisms and xenobiotics, and the fence function regulates cellular polarity. Deregulation of these functions is often observed in infectious diseases, inflammation and carcinogenesis.

Freeze-fracture electron microscopy analysis has shown that TJs are a set of continuous and anastomosing strands [3]. A series of analyses revealed that TJ-seals contain integral membrane proteins, such as occludin, claudins and junctional adhesion molecules (Fig. 1) [4–6]. The claudin protein family comprises 27 members and the junctional adhesion molecule (JAM) family comprises 3 members [4,7]. A tricellular junction-sealing component, tricellulin, has also been identified in epithelial cell sheets [8]. Occludin and tricellulin contain the tetra-spanning and other related proteins for vesicle trafficking and membrane line (MARVEL) domain. Occludin and tricellulin are members of the MARVEL protein family [9]. MarvelD3, another member of the MARVEL protein family, has been identified as a component of TJs [10]. The intracellular constituents of TJs, ZO-1 and ZO-2, determine where the claudin-based strands are formed [11]. Lipolysis-stimulated lipoprotein receptors define where tricellular junctions are formed [12]. These biochemical components of TJ-seals were all clarified within a single decade [5,6,13]. Our understanding of TJ-components has provided us with a new perspective on drug delivery and drug discovery for infectious diseases, inflammations and cancers [14–16].

There have been two main progressions in our understanding of the biology of TJs within the past 2 years: mucosal barrier homeostasis and TJ barrier homeostasis. Proof-of-concepts for TJ-targeted drug delivery have been demonstrated. In this article, we discuss recent topics in TJ biology and TJ-targeted therapy.

Biology of the epithelial barrier

Tight junctions

Epithelium is central to the construction of multicellular animals. More than 60% of the cell types in the vertebrate body are epithelial cells. Epithelia enclose and partition the animal body, line all of its surfaces and cavities, and create internal compartments. Epithelial cells are structurally polarized into a basal side that is anchored to other tissue, and an apical side that is

Corresponding author:. Kondoh, M. (masuo@phs.osaka-u.ac.jp)

1359-6446/06/$ - see front matter © 2012 Published by Elsevier Ltd. doi:10.1016/j.drudis.2012.02.014

Please cite this article in press as: A. Takahashi, et al., Pathological changes in tight junctions and potential applications into therapies, Drug Discov Today (2012), doi:10.1016/j.drudis.2012.02.014

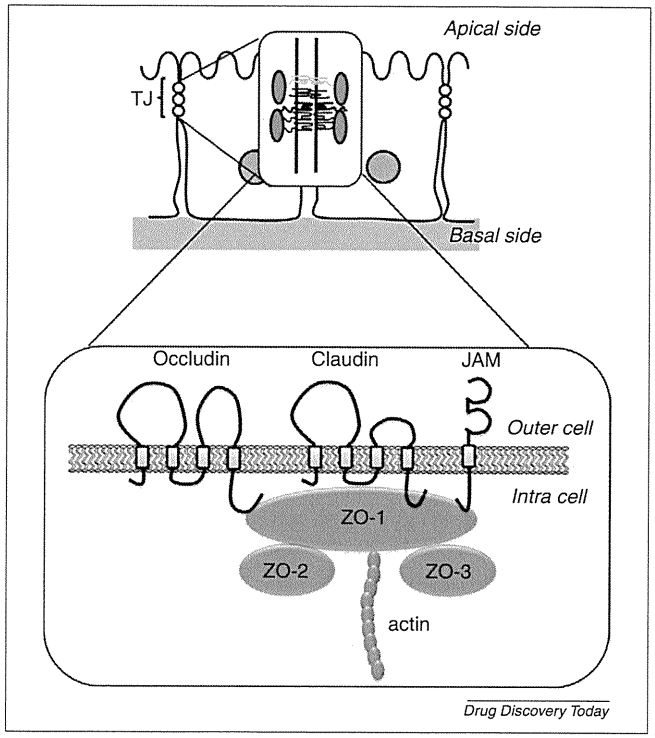

FIGURE 1

The epithelial barrier. Occludin, a tetra-transmembrane protein, was the first TJ-constituting protein identified [19]. Claudin was the second [21]. Claudins comprise a tetra-transmembrane protein family of 27 members. JAMs are glycosylated transmembrane proteins that belong to the immunoglobulin superfamily [4]. ZO-1, ZO-2 and ZO-3 are membrane-associated guanylate kinase proteins composed of a PSD95/Dlg/ZO-1 domain, an SH3 domain, a guanylate kinase domain, an acidic domain and an actin-binding region [68]. *Abbreviations*: JAMs: junctional adhesion molecules; TJ: tight junction;

unanchored. Adjacent epithelial cells are joined by occluding junctions called TJs. TJs have pivotal roles in separating the inside of the body from the outside environment, and in separating the inside and outside of tissues. TJs also function as a fence by preventing the free movement of apical membrane components and basal membrane components in epithelial cells.

TJs are intercellular sealing components located at the apical-most part of lateral membranes between adjacent epithelial cells and endothelial cells [17]. Adjacent TJ strands laterally associate with each other to form a paired strand thereby eliminating the intercellular space. Freeze fracture electron microscopy analysis revealed that TJs are continuous anastomosing intramembranous particle strands or fibrils with complementary grooves [3]. TJs are composed of transmembrane proteins, such as claudins, occludin and JAMs, in addition to cytoplasmic plaque proteins, including ZO-1, ZO-2, ZO-3 and cingulin [18].

Integral membrane proteins

Occludin was the first integral membrane protein identified in TJs [19]. Occludin has four transmembrane domains and has a molecular mass of approximately 65 kDa. Deletion of occludin does not affect the structure and function of TJs [20]. Claudins were the second integral membrane proteins identified in TJs [21]. Claudins comprise a multigene family with at least 27 members [7]. Claudins are 21–28-kDa proteins with tetratransmembrane domains. Claudins are key components in the structure and function of TJs [5,6]. A series of cellular analysis and knockout mouse analysis has clarified the roles of claudins in TJs [5,22].

Cytoplasmic proteins

ZO-1 was the first identified TJ-associated protein [23]. ZO-1, ZO-2 and ZO-3 contain PDZ-domains and the membrane-associated guanylate kinase domain. ZO-1, ZO-2 and ZO-3 are involved in formation of the TJ seal; they bind to the C-terminal cytoplasmic domain of occludin and claudins through the ZO PDZ domains [13]. ZO-1 and ZO-2 are crucial components for the definition of TJ formation [11].

Tricellular tight junctions

There are two types of TJs in epithelial cell sheets: bicellular and tricellular [2,24,25]. Occludin, claudins and JAMs are components of bicellular TJs. Tricellulin (approximately 65 kDa) is the only integral membrane component in tricellular TJs [8]. Tricellulin contains four transmembrane domains and shows structural similarity with occludin. Tricellulin is highly concentrated in tricellular TJs, but it is also localized in bicellular TJs [8,26]. Lipolysis-stimulated lipoprotein, a tricellular TJ-associated protein, defines tricellular contacts in epithelial cell sheets [12].

Mucosal barrier

The intestinal epithelium is where nutrients derived from food are absorbed, and it is also the first line of defense against microorganisms and xenobiotics. Regulation of the epithelial barrier is crucial for mucosal homeostasis. Recently, two intestinal epithelium proteins that regulate the intestinal barrier were identified.

The first protein is guanylyl cyclase C (GCC), which is a transmembrane receptor for the endogenous peptides guanylin and uroguanylin and for bacterial heat-stable enterotoxins [27]. GCC signaling has a pivotal role in the regulation of intestinal fluid and electrolyte homeostasis [28]. GCC-knockout mice show increased intestinal permeability, and GCC-knockdown in Caco-2 cells disrupts TJ integrity. This disruption of the TJ barrier is accompanied by phosphorylation of myosin II regulatory light chains, which induces TJ disassembly. GCC signaling is therefore involved in regulation of the TJ barrier [29].

The second intestinal membrane protein is matriptase. Matriptase is an integral membrane protein with trypsin-like serine protease activity and is a member of the type II transmembrane serine protease family [30]. It is widely expressed in all epithelia, and it is expressed in epithelial cells in the gastrointestinal tract [30]. Loss of matriptase reduces epithelial barrier integrity and enhances paracellular permeability. Matriptase facilitates claudin-2 loss from TJ complexes by indirect regulation of claudin-2 protein turnover by atypical protein kinase C zeta. Interestingly, matriptase does not affect some of the other TJ components, such as claudin-1, claudin-3, claudin-4, claudin-8, ZO-1, or E-cadherin [31].

These findings indicate that GCC signaling and matriptase might be potent targets for the treatment of intestinal disorders whose pathogenesis is disruption of the intestinal barrier function leading to mucosal inflammation and immune activation.

Please cite this article in press as: A. Takahashi, et al., Pathological changes in tight junctions and potential applications into therapies, Drug Discov Today (2012), doi:10.1016/j.drudis.2012.02.014

TJ dynamics

TJs are complexes of transmembrane and peripheral membrane proteins, including occludin, claudins, ZO-1 and ZO-2 [6]. The TJ structure is highly dynamic and undergoes continuous remodeling through unique kinetics [32]. The properties of TJs are determined by these dynamics [33].

Occludin S408 dephosphorylation reduces paracellular cation influx by stabilizing the occludin–ZO-1 interaction, leading to enhancement of claudin-1 and claudin-2 exchange and reduction of their pore formation at the TJ. By contrast, occludin S408 phosphorylation enhances homotypic occludin–occludin interactions, leading to the release of ZO-1 and formation of claudin-1- and claudin-2-based pores. Therefore, occludin S408 phosphorylation is a key factor in the remodeling of the claudin–occludin–ZO-1 interaction [34].

Claudin-1 is stably localized in TJs [35]. Most occludin is mobile and diffused within the junctional membrane. By contrast, most ZO-1 is continuously exchanged between the membrane and cytosol pools [34]. Fluorescence recovery after photo-bleaching (FRAP) analysis provided new insights into the dynamics of TJs. The perijunctional actomyosin ring contributes to myosin light chain kinase (MLCK)-dependent TJ regulation. FRAP analysis showed that TJ-associated ZO-1 exists in three pools: a fixed pool, a fast exchangeable pool associated with the cytosolic pool, and a slow exchangeable pool associated with the cytosolic pool. The exchange between the TJ pools and the cytosolic pool is regulated by MLCK [36]. Claudin dynamics differ depending on the particular claudin. Claudins forming TJ strands showed slower dynamics than those not forming TJ strands. Distinct claudin stabilities might affect how TJs regulate paracellular permeability by altering paracellular flux and paracellular ion permeability [37].

These insights into the dynamics of TJs address the molecular mechanism of paracellular homeostasis and will hopefully lead to the development of TJ-targeted tissue-specific and solute-specific drug delivery systems.

Epithelial barrier as the first line of defense against pathological microorganisms

The human mucosa has a surface area equivalent to 1.5 tennis courts. This large surface area means that there is significant risk of infection by pathological microorganisms; therefore, homeostasis of the epithelial barrier is important. Indeed, some pathogens modulate the epithelial barrier to facilitate easy and widespread infection (Fig. 2a).

Modulation of the epithelial barrier by pathogens

Human immunodeficiency virus-1 (HIV-1) infection is often associated with increased permeability of mucosal epithelial cells. Viral envelope glycoprotein (gp)120 is a crucial viral protein that increases the permeability of the epithelial barrier. When HIV-1 binds to cells it induces production of TNF-α, leading to a decrease in mucosal epithelial barrier integrity and spread of HIV-1 infection [38].

Atopic dermatitis (AD) is the most common inflammatory skin disease [39], and susceptibility to cutaneous infections is increased in AD patients. Widespread skin infection by the herpes simplex virus (HSV) causes severe viral complications, such as eczema herpeticum in AD patients. Defects in the epidermal TJ barrier

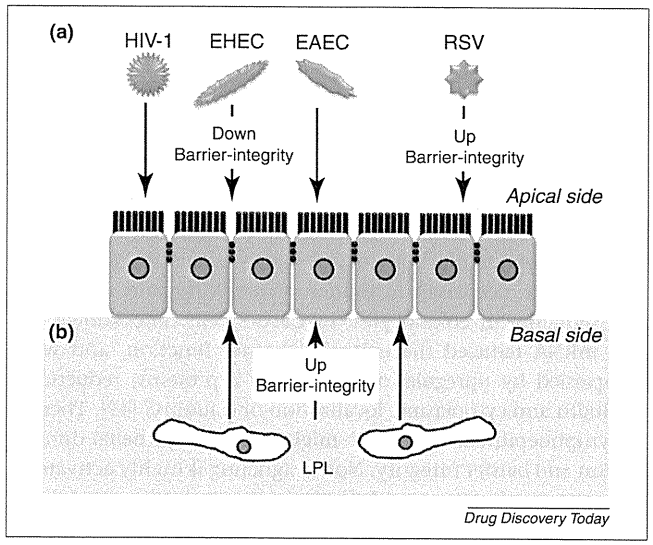

FIGURE 2

Regulation of the first line of defense, the epithelial barrier. **(a)** Pathological microorganism–epithelial barrier interaction. Infection of epithelial cells by HIV-1, EHEC, or EAEC decreased epithelial barrier integrity [38,41,42]. By contrast, RSV infection increased the barrier function [44]. **(b)** Lymphocyte–epithelial barrier interaction. LPLs regulate the integrity of the epithelial barrier via direct interaction with epithelial cells through notch signaling [49]. *Abbreviations*: EAEC: enteroaggregative *Escherichia coli*; EHEC: enterohemorrhagic *Escherichia coli*; HIV-1: human immunodeficiency virus-1; LPLs: lamina propria lymphocytes; RSV: respiratory syncytial virus.

increase the susceptibility of patients with AD to widespread subcutaneous infection with HSV or other viral pathogens [40]. In the early stage of infection with enterohemorrhagic *Escherichia coli* (EHEC), non-bloody diarrhea occurs in the absence of shiga toxin. EHEC infection increases expression of claudin-2 and redistribution of claudin-3 and occludin. These changes correlate with increased intestinal permeability [41]. Infection by enteroaggregative *Escherichia coli* (EAEC) causes dissociation of claudin-1 from the TJs between epithelial cells, leading to disruption of the TJ barrier [42]. By contrast, respiratory syncytial virus (RSV) increases TJ integrity. RSV is the major cause of bronchitis, asthma and severe lower respiratory tract diseases in infants and young children [43]. RSV infection induces expression of claudin-4 and occludin in human nasal epithelial cells. Induction of TJ components has a crucial role in epithelial cellular polarity, leading to budding of the virus from the epithelial apical surface [44]. Therefore, prevention of TJ barrier modulation by pathogens might be a viable therapeutic strategy.

Lymphoepithelial cross talk in the epithelial barrier

Mucosa-associated lymphoid tissues (MALTs) are lymphoid immune tissues that are located in the mucosal epithelium. By activating mucosal immune responses, they function as the first line of defense against pathogens invading the body through the epithelium [45]. MALTs comprise gut-associated lymphoid tissues, nasopharynx-associated lymphoid tissues and bronchus-associated lymphoid tissues. MALTs contain lymphocytes, M cells, T cells, B cells and antigen-presenting cells. Recently, lamina propria lymphocytes (LPLs) underlying the intestinal epithelium have

Please cite this article in press as: A. Takahashi, et al., Pathological changes in tight junctions and potential applications into therapies, Drug Discov Today (2012), doi:10.1016/j.drudis.2012.02.014

been shown to have a crucial role in the homeostasis of the epithelial barrier (Fig. 2b). Direct interaction of LPLs with intestinal epithelial cells is essential for the barrier function of the intestinal epithelium [46]. The notch signaling pathway regulates cell fate decisions through cell–cell interactions [47]. Notch signaling determines the differentiation of intestinal stem cells into secretory cells, absorptive cells, or enterocytes [47,48]. The absence of LPLs in mice causes increased intestinal permeability and a lack of activation of notch in colonocytes [49]. Transfer of LPLs to LPL-deficient mice decreased intestinal permeability and activated notch signaling in colonocytes. In Caco-2 cells, knockdown of notch mRNA reduced the epithelial barrier function, and was accompanied by upregulation of claudin-2 proteins, reduction of occludin and cytoplasmic localization of claudin-5 [49]. Therefore, lymphoepithelial cross talk might regulate epithelial differentiation and barrier integrity. Notch signaling is highly activated in the mucosa of patients with Crohn's disease, leading to dysregulation of the differentiation of epithelial cells [49]. Normalization of disruption of this cross talk might be a potent strategy for treating immune-mediated intestinal disorders.

Proof-of-concept for TJ-targeted drug development

As mentioned in the introduction, epithelial cells are a potent target for drug development. TJ-targeted drug development has been attempted [14,50], and proof-of-concepts for TJ-targeted drug absorption, cancer targeting and mucosal vaccination have been established. Recent findings indicate that TJ-targeted therapy for hepatitis C virus (HCV), diabetes and inflammatory diseases might be possible.

HCV infection

A total of 170 million people worldwide are infected with the HCV. Hepatitis C is the leading cause of chronic liver inflammation, cirrhosis and cancer. Claudin-1 and occludin are co-receptors for HCV infection, indicating that binders to claudin-1 or occludin might be potent inhibitors of HCV entry [16]. DNA immunization enabled successful preparation of monoclonal anti-claudin-1 antibodies against the extracellular loop of claudin-1, and these anti-claudin-1 antibodies prevented HCV infection. Antibodies effectively blocked cell entry of highly infectious escape variants of HCV that were resistant to neutralizing antibodies [51]. When hepatitis C patients reach end-stage liver failure, liver transplantation is the only choice for curative treatment; however, reinfection of the transplanted liver by HCV often occurs. There is a significant correlation between hepatic levels of claudin-1 and occludin and HCV reinfection after liver transplantation [52]. Inhibition of HCV reinfection of the transplanted liver by using anti-claudin-1 antibodies might be a potent treatment for patients with liver transplantation.

Diabetic retinopathy

Breakdown of the blood–retinal barrier (BRB) is a hallmark of diabetic retinopathy [53]. Alterations to the BRB occur early in the progression of diabetic retinopathy and eventually lead to macular edema, which is responsible for vision loss [54]. Diabetic patients show elevated levels of TNF-α in the vitreous humor. TNF-α increases the permeability of retinal endothelial cells. TNF-α decreases ZO-1 and claudin-5 expression and alters cellular localization of ZO-1 and claudin-5 [55]. Thus, regulation of BRB-integrity might be a potent strategy for treating vision loss owing to diabetes. Indeed, a chemical already in clinical use for the treatment of diabetic retinopathy, calcium dobesilate, attenuates the decrease in occludin and claudin-5 and prevents BRB breakdown [56]. Berberine, a plant alkaloid, has also been used for the treatment of diabetes. Berberine prevents barrier defects in retinal epithelial cells [57]. Inducers of occludin and claudin-5 or promoters of TJ integrity could be a potent treatment for diabetic retinopathy.

Inflammatory diseases

Berberine has been also used in the treatment of gastroenteritis and diarrhea. TNF-α disrupts TJ integrity in inflammatory bowel diseases (IBD). Regulation of the TNF-α-dependent signaling pathway is a potent strategy for the treatment of IBD. TNF-α removes claudin-1 from TJs and induces claudin-2 expression, leading to disruption of the TJ barrier. Attenuation of TNF-α signaling is a potent strategy for IBD therapy. Berberine also attenuates TNF-α-induced TJ barrier defects by removing claudin-1 and inducing claudin-2 expression [58]. Spontaneous colitis was observed in interleukin (IL)-10−/− mice in which paracellular permeability was increased in conjunction with decreased expression and redistribution of ZO-1, occludin and claudin-1. Treatment with a probiotic, *Lactobacillus plantarum*, restored expression of TJ components and TJ integrity, resulting in prevention of bacterial translocation and proinflammatory responses in IL-10−/− mice [59]. Recovery of TJ integrity might be a potent strategy for inflammatory intestinal diseases. Ouabain, which is an inhibitor of Na^+, K^+-ATPase, increased TJ integrity through signaling pathways involving c-Src and ERK1/2 and by modulating the expression of claudin-1, claudin-2 and claudin-4 [60,61]. Several natural products have been found to be therapeutically useful against epithelial barrier defects.

Paracellular drug transport

The claudin protein family comprises 27 members [7]. Claudins form homo- and hetero-type strands in the lateral membrane. Adjacent claudin-based TJ strands associate with each other, leading to sealing of the intercellular space. The combination of the claudin members is a determinant factor for the properties of the TJ barrier [5]. These findings suggest that optimization of claudin modulators with narrow-specificity in certain cases, or broad-specificity in other cases, might regulate solute- and tissue-specificity in paracellular transport. The most important issue in TJ-targeted drug absorption is the development of claudin modulators. Claudin is an integral membrane protein with a tetra-transmembrane domain. Claudin binders are the first choice for claudin modulators. The first extracellular loop contains approximately 50 amino acids and the second contains approximately ten amino acids. Claudins are hydrophobic proteins, and preparation of a recombinant protein is only currently possible for claudin-4 [62]. Therefore, the development of claudin binders, including antibodies, has been slow. Budded baculoviruses display functional forms of membrane proteins on their surface [63]. Claudin-displaying budded baculoviruses possess a native form of claudin and can be used as a screening system for claudin binders [64]. Functional membrane proteins are heterogeneously expressed on

Please cite this article in press as: A. Takahashi, et al., Pathological changes in tight junctions and potential applications into therapies, Drug Discov Today (2012), doi:10.1016/j.drudis.2012.02.014

budded baculoviruses [63]. Functional information using FRAP analysis will enable development of a screening system for claudin modulators with narrow- or broad-specificity using the heterogenous claudin-displaying baculoviral system. We predict that, in the near future, proof-of-concept for tissue- and solute-specific paracellular transport by modulating the claudin-barrier will be demonstrated.

Coupling of transcellular and paracellular transport systems controls permeability to solutes [65]. Claudin-based TJs function as charge-selective paracellular channels [6]. Claudin-15 is responsible for transepithelial permeability to extracellular monovalent cations, especially Na^+. Claudin-15-deficient mice exhibit low luminal Na^+ levels and low glucose absorption in the intestine, indicating that paracellular transport of Na^+ through claudin-15-based TJ strands might be coupled to transcellular transport of glucose through a glucose transporter [66]. These findings suggest that modulation of the claudin-mediated paracellular transport of solutes might regulate the transcellular transport of drugs through a transporter.

Concluding remarks

To our knowledge, the first report of TJ-targeted drug development was the discovery in 1961 of enhanced mucosal absorption of drugs by co-administration of ethylenediaminetetraacetic acid [67]. TJs were identified in 1963 [17]. Modulation of the TJ-barrier has been a major strategy for enhancing mucosal absorption; however, the biochemical structure of TJs was unclear until 1998. Until that year, absorption enhancers were screened mainly by modulating epithelial cell sheets. Recent imaging studies have begun to reveal the dynamics of TJs and also how these dynamics are regulated [36,37]. Future detailed analyses using FRAP will provide us with new insights into strategies for modulation of the TJ barrier. In addition to TJ-modulated drug absorption, TJ-targeted therapy for HCV infection and diabetic retinopathy has recently been proved effective [51,56]. The questions of how TJ dynamics are regulated, and how expression of TJ components is regulated are still to be answered. The molecular pathology of deregulation of the TJ barrier is not yet fully understood. TJ-targeted drug development has been spearheaded by rapid progress in our understanding of the biology of the TJ barrier.

Acknowledgements

This work was supported in part by a Grant-in-Aid for Scientific Research from the Ministry of Education, Culture, Sports, Science and Technology, Japan (21689006) and by Health and Labor Sciences Research Grants from the Ministry of Health, Labor and Welfare of Japan. AT and HS are supported by Research Fellowships of the Japan Society for the Promotion of Science for Young Scientists.

References

1 Anderson, J.M. and Van Itallie, C.M. (1995) Tight junctions and the molecular basis for regulation of paracellular permeability. *Am. J. Physiol.* 269 (4 Pt 1), G467–G475
2 Gumbiner, B. (1993) Breaking through the tight junction barrier. *J. Cell Biol.* 123, 1631–1633
3 Staehelin, L.A. (1973) Further observations on the fine structure of freeze-cleaved tight junctions. *J. Cell Sci.* 13, 763–786
4 Chiba, H. *et al.* (2008) Transmembrane proteins of tight junctions. *Biochim. Biophys. Acta* 1778, 588–600
5 Furuse, M. and Tsukita, S. (2006) Claudins in occluding junctions of humans and flies. *Trends Cell Biol.* 16, 181–188
6 Van Itallie, C.M. and Anderson, J.M. (2009) Physiology and function of the tight junction. *Cold Spring Harb. Perspect. Biol.* 1, a002584
7 Mineta, K. *et al.* (2011) Predicted expansion of the claudin multigene family. *FEBS Lett.* 585, 606–612
8 Ikenouchi, J. *et al.* (2005) Tricellulin constitutes a novel barrier at tricellular contacts of epithelial cells. *J. Cell Biol.* 171, 939–945
9 Sanchez-Pulido, L. *et al.* (2002) MARVEL: a conserved domain involved in membrane apposition events. *Trends Biochem. Sci.* 27, 599–601
10 Raleigh, D.R. *et al.* (2010) Tight junction-associated MARVEL proteins marvelD3, tricellulin, and occludin have distinct but overlapping functions. *Mol. Biol. Cell* 21, 1200–1213
11 Umeda, K. *et al.* (2006) ZO-1 and ZO-2 independently determine where claudins are polymerized in tight-junction strand formation. *Cell* 126, 741–754
12 Masuda, S. *et al.* (2011) LSR defines cell corners for tricellular tight junction formation in epithelial cells. *J. Cell Sci.* 124 (Pt 4), 548–555
13 Furuse, M. (2010) Molecular basis of the core structure of tight junctions. *Cold Spring Harb. Perspect. Biol.* 2, a002907
14 Takahashi, A. *et al.* (2011) Claudin as a target for drug development. *Curr. Med. Chem.* 18, 1861–1865
15 Turksen, K. and Troy, T.C. (2011) Junctions gone bad: claudins and loss of the barrier in cancer. *Biochim. Biophys. Acta* 1816, 73–79
16 Zeisel, M.B. *et al.* (2011) Hepatitis C virus entry into hepatocytes: molecular mechanisms and targets for antiviral therapies. *J. Hepatol.* 54, 566–576
17 Farquhar, M.G. and Palade, G.E. (1963) Junctional complexes in various epithelia. *J. Cell Biol.* 17, 375–412
18 Nusrat, A. *et al.* (2000) Molecular physiology and pathophysiology of tight junctions. IV. Regulation of tight junctions by extracellular stimuli: nutrients, cytokines, and immune cells. *Am. J. Physiol.* 279, G851–G857
19 Furuse, M. *et al.* (1993) Occludin: a novel integral membrane protein localizing at tight junctions. *J. Cell Biol.* 123 (6 Pt 2), 1777–1788
20 Saitou, M. *et al.* (1998) Occludin-deficient embryonic stem cells can differentiate into polarized epithelial cells bearing tight junctions. *J. Cell Biol.* 141, 397–408
21 Furuse, M. *et al.* (1998) A single gene product, claudin-1 or -2, reconstitutes tight junction strands and recruits occludin in fibroblasts. *J. Cell Biol.* 143, 391–401
22 Furuse, M. (2009) Knockout animals and natural mutations as experimental and diagnostic tool for studying tight junction functions *in vivo*. *Biochim. Biphys. Acta* 1788, 813–819
23 Stevenson, B.R. *et al.* (1986) Identification of ZO-1: a high molecular weight polypeptide associated with the tight junction (zonula occludens) in a variety of epithelia. *J. Cell Biol.* 103, 755–766
24 Staehelin, L.A. *et al.* (1969) Freeze-etch appearance of the tight junctions in the epithelium of small and large intestine of mice. *Protoplasma* 67, 165–184
25 Friend, D.S. *et al.* (1972) Variations in tight and gap junctions in mammalian tissues. *J. Cell Biol.* 53, 375–412
26 Ikenouchi, J. *et al.* (2008) Loss of occludin affects tricellular localization of tricellulin. *Mol. Biol. Cell* 19, 4687–4693
27 Lin, J.E. *et al.* (2009) Guanylyl cyclase C in colorectal cancer: susceptibility gene and potential therapeutic target. *Future Oncol.* 5, 509–522
28 Lorenz, J.N. *et al.* (2003) Uroguanylin knockout mice have increased blood pressure and impaired natriuretic response to enteral NaCl load. *J. Clin. Invest.* 112, 1244–1254
29 Han, X. *et al.* (2011) Loss of guanylyl cyclase C (GCC) signaling leads to dysfunctional intestinal barrier. *PLoS ONE* 6, E16139
30 Bugge, T.H. *et al.* (2007) Matriptase-dependent cell surface proteolysis in epithelial development and pathogenesis. *Front. Biosci.* 12, 5060–5070
31 Buzza, M.S. *et al.* (2010) Membrane-anchored serine protease matriptase regulates epithelial barrier formation and permeability in the intestine. *Proc. Natl. Acad. Sci. U. S. A.* 107, 4200–4205
32 Ikenouchi, J. *et al.* (2003) Regulation of tight junctions during the epithelium–mesenchyme transition: direct repression of the gene expression of claudins/occludin by Snail. *J. Cell Sci.* 116 (Pt 10), 1959–1967
33 Steed, E. *et al.* (2010) Dynamics and functions of tight junctions. *Trends Cell Biol.* 20, 142–149
34 Raleigh, D.R. *et al.* (2011) Occludin S408 phosphorylation regulates tight junction protein interactions and barrier function. *J. Cell Biol.* 193, 565–582

Please cite this article in press as: A. Takahashi, et al., Pathological changes in tight junctions and potential applications into therapies, Drug Discov Today (2012), doi:10.1016/j.drudis.2012.02.014

35 Sasaki, H. *et al.* (2003) Dynamic behavior of paired claudin strands within apposing plasma membranes. *Proc. Natl. Acad. Sci. U. S. A.* 100, 3971–3976
36 Yu, D. *et al.* (2010) MLCK-dependent exchange and actin binding region-dependent anchoring of ZO-1 regulate tight junction barrier function. *Proc. Natl. Acad. Sci. U. S. A.* 107, 8237–8241
37 Yamazaki, Y. *et al.* (2011) Role of claudin species-specific dynamics in reconstitution and remodeling of the zonula occludens. *Mol. Biol. Cell* 22, 1495–1504
38 Nazli, A. *et al.* (2010) Exposure to HIV-1 directly impairs mucosal epithelial barrier integrity allowing microbial translocation. *PLoS Pathog.* 6, E1000852
39 Beck, L.A. *et al.* (2009) Phenotype of atopic dermatitis subjects with a history of eczema herpeticum. *J. Allergy Clin. Immunol.* 124, 260–269 269 E261–E267
40 De Benedetto, A. *et al.* (2011) Reductions in claudin-1 may enhance susceptibility to herpes simplex virus 1 infections in atopic dermatitis. *J. Allergy Clin. Immunol.* 128, 242–246 E245
41 Roxas, J.L. *et al.* (2010) Enterohemorrhagic *E. coli* alters murine intestinal epithelial tight junction protein expression and barrier function in a Shiga toxin independent manner. *Lab. Invest.* 90, 1152–1168
42 Strauman, M.C. *et al.* (2010) Enteroaggregative *Escherichia coli* disrupts epithelial cell tight junctions. *Infect. Immun.* 78, 4958–4964
43 Bitko, V. and Barik, S. (1998) Persistent activation of RelA by respiratory syncytial virus involves protein kinase C, underphosphorylated IkappaBbeta, and sequestration of protein phosphatase 2A by the viral phosphoprotein. *J. Virol.* 72, 5610–5618
44 Masaki, T. *et al.* (2011) A nuclear factor-kappaB signaling pathway via protein kinase C delta regulates replication of respiratory syncytial virus in polarized normal human nasal epithelial cells. *Mol. Biol. Cell* 22, 2144–2156
45 Kunisawa, J. *et al.* (2008) Immunological commonalities and distinctions between airway and digestive immunity. *Trends Immunol.* 29, 505–513
46 Dahan, S. *et al.* (2009) Lymphoepithelial interactions: a new paradigm. *Ann. N. Y. Acad. Sci.* 1165, 323–326
47 Kopan, R. and Ilagan, M.X. (2009) The canonical Notch signaling pathway: unfolding the activation mechanism. *Cell* 137, 216–233
48 Hermiston, M.L. *et al.* (1993) Chimeric-transgenic mice represent a powerful tool for studying how the proliferation and differentiation programs of intestinal epithelial cell lineages are regulated. *Proc. Natl. Acad. Sci. U. S. A.* 90, 8866–8870
49 Dahan, S. *et al.* (2011) Notch-1 signaling regulates intestinal epithelial barrier function, through interaction with $CD4^+$ T cells, in mice and humans. *Gastroenterology* 140, 550–559
50 Kondoh, M. *et al.* (2008) Targeting tight junction proteins – significance for drug development. *Drug Discov. Today* 13, 180–186
51 Fofana, I. *et al.* (2010) Monoclonal anti-claudin 1 antibodies prevent hepatitis C virus infection of primary human hepatocytes. *Gastroenterology* 139, 953–964 964 E951–E954
52 Mensa, L. *et al.* (2011) Hepatitis C virus receptors claudin-1 and occludin after liver transplantation and influence on early viral kinetics. *Hepatology* 53, 1436–1445
53 Cunha-Vaz, J. *et al.* (1975) Early breakdown of the blood–retinal barrier in diabetes. *Br. J. Ophthalmol.* 59, 649–656
54 The Diabetes Control and Complications Trial Research Group, (1993) The effect of intensive treatment of diabetes on the development and progression of long-term complications in insulin-dependent diabetes mellitus. *N. Engl. J. Med.* 329, 977–986
55 Aveleira, C.A. *et al.* (2010) TNF-alpha signals through PKCzeta/NF-kappaB to alter the tight junction complex and increase retinal endothelial cell permeability. *Diabetes* 59, 2872–2882
56 Leal, E.C. *et al.* (2010) Calcium dobesilate inhibits the alterations in tight junction proteins and leukocyte adhesion to retinal endothelial cells induced by diabetes. *Diabetes* 59, 2637–2645
57 Cui, H.S. *et al.* (2007) Effect of berberine on barrier function in a human retinal pigment epithelial cell line. *Jpn. J. Ophthalmol.* 51, 64–67
58 Amasheh, M. *et al.* (2010) TNFalpha-induced and berberine-antagonized tight junction barrier impairment via tyrosine kinase, Akt and NFkappaB signaling. *J. Cell Sci.* 123 (Pt 23), 4145–4155
59 Chen, H.Q. *et al.* (2010) Lactobacillus plantarum ameliorates colonic epithelial barrier dysfunction by modulating the apical junctional complex and PepT1 in IL-10 knockout mice. *Am. J. Physiol.* 299, G1287–G1297
60 Larre, I. *et al.* (2010) Ouabain modulates epithelial cell tight junction. *Proc. Natl. Acad. Sci. U. S. A.* 107, 11387–11392
61 Larre, I. *et al.* Ouabain modulates ciliogenesis in epithelial cells. *Proc. Natl. Acad. Sci. U. S. A.*, doi:10.1073/pnas.1102617108 (in press)
62 Mitic, L.L. *et al.* (2003) Expression, solubilization, and biochemical characterization of the tight junction transmembrane protein claudin-4. *Protein Sci.* 12, 218–227
63 Sakihama, T. *et al.* (2008) Functional reconstitution of G-protein-coupled receptor-mediated adenylyl cyclase activation by a baculoviral co-display system. *J. Biotechnol.* 135, 28–33
64 Kakutani, H. *et al.* (2011) A novel screening system for claudin binder using baculoviral display. *PLoS ONE* 6, E16611
65 Kapus, A. and Szaszi, K. (2006) Coupling between apical and paracellular transport processes. *Biochem. Cell Biol.* 84, 870–880
66 Tamura, A. *et al.* (2011) Loss of claudin-15, but not claudin-2, causes Na(+) deficiency and glucose malabsorption in mouse small intestine. *Gastroenterology* 140, 913–923
67 Windsor, E. and Cronheim, G.E. (1961) Gastro-intestinal absorption of heparin and synthetic heparinoids. *Nature* 190, 263–264
68 Gonzalez-Mariscal, L. *et al.* (2000) MAGUK proteins: structure and role in the tight junction. *Semin. Cell Dev. Biol.* 11, 315–324

Please cite this article in press as: A. Takahashi, et al., Pathological changes in tight junctions and potential applications into therapies, Drug Discov Today (2012), doi:10.1016/j.drudis.2012.02.014

Journal of Bioscience and Bioengineering
VOL. 111 No. 5, 597–599, 2011

www.elsevier.com/locate/jbiosc

Modifying the antigen-immunization schedule improves the variety of monoclonal antibodies obtained from immune-phage antibody libraries against HIV-1 Nef and Vif

Mai Yoshikawa,[1,†] Yohei Mukai,[1,†] Shin-ichi Tsunoda,[2] Yasuo Tsutsumi,[1,2] Yasuo Yoshioka,[1,3] Naoki Okada,[1] and Shinsaku Nakagawa[1,*]

Department of Biotechnology and Therapeutics, Graduate School of Pharmaceutical Sciences, Osaka University, 1–6 Yamadaoka, Suita, Osaka 565–0871, Japan,[1] Laboratory of Biopharmaceutical Research, National Institute of Biomedical Innovation (NiBio), Osaka 567-0085, Japan,[2] and The Center for Advanced Medical Engineering and Informatics, Osaka University, 1–6 Yamadaoka, Suita, Osaka 565–0871, Japan[3]

Received 2 August 2010; accepted 25 December 2010
Available online 28 January 2011

Immune phage antibody libraries are an attractive technology for isolating antigen-specific monoclonal antibodies (mAbs). Here we show that the immunization schedule affects the immune phage antibody library properties. We subcutaneously (s.c.) administered HIV-1 Nef and Vif antigens with different schedules (25 μg×2 s.c. and 10 μg×3 s.c.). The variety of isolated mAbs in 25 μg×2 s.c. groups (Nef: 11 clones, Vif: 9 clones) was superior to that in the 10 μg×3 s.c. groups (Nef: 2 clones, Vif: 1 clone). This finding suggests that it is important to optimize the immunization schedule for isolating a wide variety of mAbs.
© 2011, The Society for Biotechnology, Japan. All rights reserved.

[**Key words:** Phage display system; Monoclonal antibody; HIV-1; Antibody library; Immunization; Drug delivery; Targeting; Antibody therapy]

Phage antibody libraries are an extremely attractive technology that enables rapid isolation of monoclonal antibodies (mAbs) toward the development of therapeutic agents and basic research tools (1). Immune phage antibody library, constructed from cDNA derived from B-cells in the spleen of immunized animals, in particular, allows for an isolation of the desired mAbs with high antigen affinity and specificity (2). This library contains the antibody repertories reconstructed from B-cells of immunized animals. Therefore, the diversity of the antigen specific B-cell repertory is important to obtain a large variety of the desired mAbs. In general, after immunization, activated B-cells individually produce antigen-specific mAbs. Excess immunization, however, enhances the survival of specific B-cells that express mAbs with high affinities to antigens, resulting in a limited antigen-specific B-cell repertory in immunized animals (3). To obtain a large variety of mAbs, optimizing the strength of the immunization is promising to retain the diversity of antigen specific B-cells in vivo.

A large variety of antigen-specific mAbs is preferable for developing therapeutic agents as well as for many applications in basic research (4,5). In particular, certain types of mAbs, such as neutralizing mAbs, signaling mAbs, and intracellular mAbs (intrabody), are useful, but difficult to obtain because of their rarity. These specialized mAbs must be screened from various candidate mAbs (6). Therefore, a method to identify a large variety of mAbs is highly desirable to accelerate the discovery of specialized mAbs.

HIV-1 encoded Nef and Vif proteins have an important role in HIV-1 viral replication and infectivity (7). Computer-based drug design against HIV enzymes has been successfully achieved, but is not adequate for complete therapy because of some drug resistance. HIV-1 Nef and Vif are also considered attractive targets for anti-HIV therapy. Computer-based drug design for Nef and Vif is also difficult, however, because these targets do not have a clear active domain for the design of specific drug-like enzymes. Therefore, it is thought that intrabody-based therapy will be a promising approach for therapy against these proteins (7,8). A large variety of mAbs will be necessary, however, to isolate the intrabody that can inhibit the viral activity of HIV.

Here we analyzed a variety of single-chain antibody variable domain fragments (scFvs) obtained from different immunization schedules in the scFv phage display using Nef and Vif antigens. We immunized mice with Nef or Vif using different protocols and assessed the amplification efficiency of their genes of variable domains (V genes). We then constructed anti-Nef and anti-Vif scFv phage libraries and estimated the variety of scFvs obtained from these phage libraries. The findings of the present study provide critical information to enable isolation of a wide variety of mAbs from immune phage antibody libraries. These findings will also contribute to the discovery of specialized mAbs useful for both future therapies and advanced basic research.

MATERIALS AND METHODS

Immunization with Nef and Vif recombinant protein On day 0, 6-week-old female BALB/c mice were subcutaneously (s.c.) injected with 25 μg or 10 μg of antigens as 100-μl emulsions with a Titer Max Gold adjuvant (Sigma-Aldrich Corp., St. Louis, MO, USA). For these immunizations, we used purified recombinant HIV-1 Nef and HIV-1 Vif proteins

* Corresponding author. Tel.: +81 6 6879 8175; fax: +81 6 6879 8179.
E-mail addresses: yohe@phs.osaka-u.ac.jp (Y. Mukai), nakagawa@phs.osaka-u.ac.jp (S. Nakagawa).
† The first two authors contributed equally to this work.

1389-1723/$ - see front matter © 2011, The Society for Biotechnology, Japan. All rights reserved.
doi:10.1016/j.jbiosc.2010.12.025

(Immunodiagnostics, Inc., Woburn, MA) as antigens. On day 14, the immunizations were repeated in the same manner. The group administered with 10 μg received an additional immunization on day 28. Serum samples were collected on days 14, 21, and 35, and IgG titers were measured using Nef- or Vif-immobilized capture ELISA.

Calculation of antibody titer in collected serum Nef or Vif recombinant protein (Immunodiagnostics, Inc.) was immobilized on immunoassay plates (Nalge Nunc International, Rochester, NY, USA) at 4°C for 8 h. The plates were blocked with 4% Block Ace (Dainippon Sumitomo Pharma Co., Ltd, Osaka, Japan) at 37°C for 2 h. Serum samples were diluted with 0.4% Block Ace, and then reacted with immobilized antigens for 1 h at room temperature. Anti-mouse IgG horseradish peroxidase (HRP) conjugate (Sigma-Aldrich Corp.) was reacted for 1 h at room temperature, and then HRP activity was assessed by a 3,3′,5,5′-tetramethylbenzidine (TMB) substrate (Thermo Fisher Scientific Inc., Rockford, IL, USA). The reaction was stopped by 1 N H_2SO_4, and then absorbance was measured at 450 nm and 655 nm as a reference. Antibody titers were calculated as Log_2 titer. Log_2 titer indicates a maximum serum dilution value (2^n) that can induce the antigen-specific binding potency.

Construction of the phage antibody library Immunized mice were killed on day 21 (25 μg×2 s.c. groups) or on day 35 (10 μg×3 s.c. groups). Spleen and bone marrow cells were collected separately from immunized mice. The phage antibody library was constructed as described previously (9) with a slight modification. Briefly, variable regions of immunoglobulin light-chain (VL) and heavy-chain (VH) genes were amplified by polymerase chain reaction (PCR) using an original primer set (9). VL and VH cDNAs were linked by PCR to synthesize the scFv gene library. The cDNAs were amplified by the following primers: Y15-2 (5′-GTTCCTTTCTATGCGGCCCAGCCGGC-CATGGCC-3′) and Y16-2 (5′-ATCCGGATACGGCACCGGCGCACCTGCGGCCGC-3′) by cycling 35 times at 96°C for 60 s, 65°C for 60 s, and 68°C for 60 s. The amplified scFv gene library was digested by *Nco* I and *Not* I, and then cloned into pCANTAB5E. The products were transformed into *E. coli* TG1 strain, and these TG1 cells were used in the phage preparation. The library size was estimated from the number of colonies formed in this transformation. Preparation of the phage library was described previously (9).

Affinity panning Anti-FLAG M2 antibody (Sigma-Aldrich Corp.) and Nef and Vif recombinant protein (Immunodiagnostics, Inc.) were immobilized on immunoassay plates (Nalge Nunc International) at 4°C for 8 h. The plates were blocked by 10% skim milk (Becton Dickinson and Company, Franklin Lakes, NJ, USA) containing 25% glycerol at 37°C for 2 h. Each phage library was reacted with an immobilized anti-FLAG M2 antibody for 1 h at 4°C. After washing with 0.05% Tween 20 (Sigma-Aldrich Corp.), the FLAG-positive phages were rescued using 20 mM glycine-HCl buffer (pH = 2.0), and then neutralized in a 1 M Tris-HCl buffer (pH = 8.0). The eluent was reacted with immobilized Nef or Vif protein for 1 h at 4°C. The antigen-binding phages were rescued by 0.1 N HCl, and then neutralized in a 1 M Tris-HCl buffer (pH = 8.0). The obtained phages were amplified by infecting to the exponential growth of TG1. This panning step was repeated five times. The phage titer was measured by counting the number of colonies on Petrifilm™ *E. coli* count plates (3M Company, Two Harbors, MN, USA).

Phage ELISA One hundred fifty TG1 colonies were picked up from the plates after each panning. They were grown in 96-well plates at 37°C, and then monoclonal phages were produced from each TG1 by the infection of M13KO7 helper phages. The amplified phages were then blocked with 2% Block Ace (Dainippon Sumitomo Pharma Co.) at 4°C for 1 h and then added to an immunoassay plate coated with the antigens. Plates were then incubated for 1 h, with agitation at 250 rpm, and washed three times with phosphate buffered saline/0.1% Tween 20, and finally incubated with HRP-conjugated anti-M13 monoclonal antibody (Amersham Bioscience). HRP activity was assessed by the TMB substrate (MOSS, Inc.). The reaction was stopped by 1 N H_2SO_4, and then the absorbance was measured at 450 nm and 655 nm as a reference.

RESULTS

Amplification of the VL and VH gene libraries Mice were immunized with HIV-1 Nef or Vif antigens at 10 μg or 25 μg each. Antibody induction was observed after the 2nd immunization (Table 1, day 21). The mice receiving 25 μg were killed on day 21 (25 μg×2 s.c. group). Because the antibody titers of mice receiving 10 μg were not sufficient, we performed a 3rd immunization in mice administered with 10 μg. After the 3rd immunization, sufficient antibody titers were observed in the groups receiving 10 μg (Table 1, day 35) and then the mice were killed on day 35 (10 μg×3 s.c. group).

TABLE 1. Antibody titers induced in Nef or Vif-immunized mice.

Antigen	Dose	Log_2 titer (2^n)		
		Day 14	Day 21	Day 35
Nef	10 μg	<6	9	13
	25 μg	<6	12	N.T.
Vif	10 μg	<6	10	13
	25 μg	<6	12	N.T.

Nef or Vif recombinant antigen (10 μg or 25 μg) was injected into 5 mice on day 0. On day 14, the same dose of antigen was injected into the same mice. For the 10-μg immunization groups, an additional immunization was performed on day 28. Antigen titers from the collected serum on days 14, 21, and 35 were measured by ELISA. Log_2 titer indicates maximum serum dilution value (2^n) that can induce the antigen specific binding potency. N.T., not tested.

The VL and VH genes were amplified from cDNA derived from the spleens and bone marrow cells of immunized mice using a primer mix including thousands of independent primers (9). In both immunizations of Nef and Vif, the amplifications of V genes were more efficient in the 25 μg×2 s.c. groups than in the 10 μg×3 s.c. groups (Fig. 1). The yields of V genes in the 25 μg×2 s.c. groups were approximately 10 times higher than those in the 10 μg×3 s.c. groups. In each group, VH and VL genes were linked by PCR, and then the obtained scFv genes were ligated in the pCANTAB5E vector.

Quality checks of immune scFv phage libraries These plasmid libraries were transformed into TG1, and the diversity of library was estimated from the number of colonies formed in the transformation. Each library contained a 200 to 700 million scFv repertory. DNA sequence analysis of 20 clones picked randomly from each library indicated that each library comprised independent clones with different sequences (data not shown). We produced phage antibody libraries from these TG1s, and then evaluated the affinity of each phage library against each antigen by phage ELISA. The results suggested that both phage libraries from mice immunized with Nef had almost the same affinity against the immobilized Nef (Fig. 2A). Similar results were obtained in the anti-Vif phage libraries (Fig. 2B). The results suggested that the whole affinity of each phage library did not depend on the immunization schedule. These results are also consistent with the results of the antibody values in the serums shown in Table 1.

Selection and identification of the antigen-specific scFvs Anti-Nef or anti-Vif scFv displaying phages were concentrated by repeating the affinity panning against Nef or Vif, respectively. The output/input ratios were increased similarly in all groups during 5 panning steps (Figs. 3A, B). The output/input ratio indicates the concentration of the phages displaying anti-Nef or anti-Vif scFvs. The results showed that the efficiency in concentrating the desired phages also did not depend on their immunization schedules.

To identify antigen-specific scFvs, 150 colonies were randomly picked up after the 3rd, 4th, and 5th panning. The affinities of monoclonal phages against Nef or Vif were then assessed by phage ELISA. Many scFvs showed antigen-specific affinity in all groups. We picked up clones with the antigen-specific affinity, and then confirmed their sequences to analyze the variety of the obtained scFvs. From the 25 μg×2 s.c. groups, we could identify different scFvs (11 scFvs for Nef and 9 scFvs for Vif) (Table 2). On the other hand, from the 10 μg×3 s.c. groups, the variety of the obtained scFvs was extremely limited (2 scFvs for Nef and 1 scFv for Vif) (Table 2). We also confirmed that scFvs from

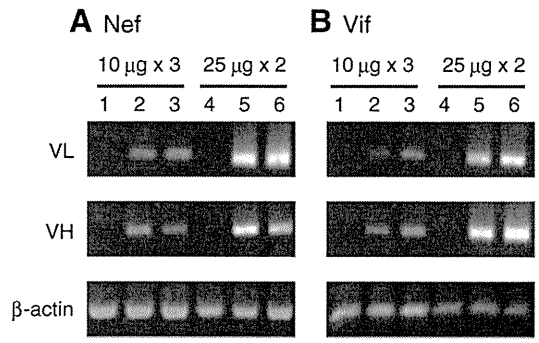

FIG. 1. Amplification of VL and VH gene repertories from Nef or Vif-immunized mice. VL and VH gene repertories were amplified from cDNAs that were synthesized from spleen and bone marrow-derived mRNAs from Nef or Vif-immunized mice. VL and VH genes were obtained by PCR from 1 μl of (A) Nef or (B) Vif-immunized mice cDNA using 1 μl (Lanes 1 and 4); 2 μl (Lanes 2 and 5); or 4 μl (Lanes 3 and 6) of our original mix primers. β-Actin gene was amplified with the same protocol as a positive control.

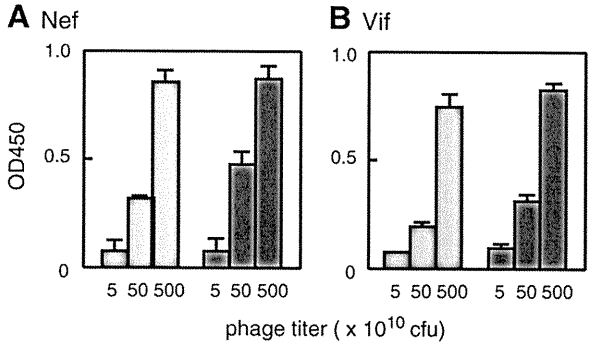

FIG. 2. The binding potency of Nef or Vif immunized phage libraries. The binding potency of the Nef (A) or Vif (B) immunized phage library was evaluated by phage ELISA against immobilized Nef or Vif recombinant antigen, respectively. Phage libraries constructed from mice immunized with 10 μg antigen ×3 (grey column) or 25 μg antigen ×2 (black column) were used in this experiment. 5×10^{10} –5×10^{12} colony forming unit (cfu) phage solutions were added to the immobilized antigens and detected by horseradish peroxidase-linked anti-M13 antibody.

the 10 μg×3 s.c. groups were included in the 25 μg×2 s.c. groups. The obtained scFvs were all identified after the 3rd panning, and the variety of scFvs was decreased during the 4th and 5th panning (Table 2). These results suggested that phage libraries in the 25 μg×2 s.c. groups had a greater diversity of scFvs than those in the 10 μg×3 s.c. groups.

DISCUSSION

These findings of the present study indicated that the diversity of antigen specific antibodies displayed on a phage library greatly depended on the immunization protocol. In the immunization, antibody values in the serums of 10 μg×3 s.c. and 25 μg×2 s.c. groups were similar, but the efficiencies of the amplification in the 25 μg×2 s.c. groups were greater than those in the 10 μg×3 s.c. groups. In this step, we used a mixture of primers to amplify almost all antibody repertoires (9). Therefore, these results indicated that the diversity of antibody-producing B-cells in the 10 μg×3 s.c. groups was extremely limited. Indeed, after the selections, we obtained only 2 anti-Nef scFvs and 1 anti-Vif scFv in the 10 μg×3 s.c. groups despite obtaining 11 anti-Nef scFvs and 9 anti-Vif scFvs in the 25 μg×2 s.c. groups. A previous report showed that increased immunization frequency and timespan enhance the survival of B-cells that express the antibody with high affinity, resulting in a small antibody repertory in immunized animals (3). Our result showed that this machinery is also important for the construction of an immune phage antibody library, and the induction of a high antibody titer in a short

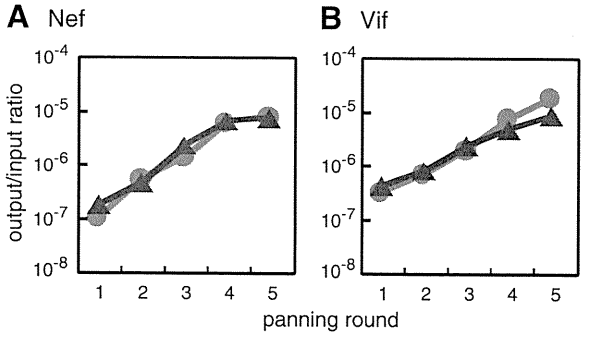

FIG. 3. Concentration of anti-Nef or Vif mAb displaying phages by affinity panning. Anti-Nef or Vif scFv-displaying phages were concentrated by affinity panning against immobilized Nef or Vif recombinant antigens, respectively. The output/input ratio (output phage titer/input phage titer) of the (A) Nef- or (B) Vif-immunized library was calculated and plotted. Grey circles indicate the output/input ratio of the 10 μg×3 s.c. groups, and black triangles indicate that of the 25 μg×2 s.c. groups.

TABLE 2. The diversity of isolated scFvs from each phage antibody library.

Antigen		Nef		Vif	
Dose		10 μg	25 μg	10 μg	25 μg
Clones	3rd	2	11	1	9
	4th	1	3	1	3
	5th	1	1	1	1
	Unique	2	11	1	9

One hundred fifty clones were randomly picked from 3rd, 4th, and 5th panning output repertories. The binding potencies of these clones were assessed by phage ELISA. The variety of isolated clones was assessed by sequencing positive clones in phage ELISA after each panning round. "Unique" indicates the variety of unique clones obtained from through 3rd to 5th panning.

period will be helpful to obtain the large variety of antibodies from an immune phage antibody library.

Nef and Vif, the model targets in this study, are attractive targets for anti-HIV therapy in HIV-infected T-cells (7). Antibodies that can work in the cell are known as intrabodies, which have recently received a lot of attention (10). To target these intracellular molecules, it is necessary to isolate antibodies that fold and function properly in a reduced intracellular environment (11). Because these antibodies are rare, however, it is important to screen from high variety of antibodies that recognize the same target. From this point of view, anti-Nef and anti-Vif scFvs identified in this report will be useful as intrabody candidates.

In conclusion, the immunization protocol affects the variety of antibodies identified from phage antibody libraries. We expect that our findings will allow for the isolation of a large variety of antibodies that will be helpful for screening any desired antibodies and contribute to the progress of biotechnology for the development of antibody-based medicine and other basic protein research.

ACKNOWLEDGMENTS

This study was supported by Research Fund Project on Health Sciences focusing on Drug Innovation from the Japan Health Sciences Foundation, and in part by a Grant-in-Aid for Scientific research (B) and Grant-in-Aid for Scientific Research on Innovative Areas and from the Ministry of Education, Culture, Sports, Science, and Technology of Japan (MEXT) and Japan Society for the Promotion of Science (JSPS).

References

1. **McCafferty, J., Griffiths, A. D., Winter, G., and Chiswell, D. J.:** Phage antibodies: filamentous phage displaying antibody variable domains, Nature, **348**, 552–554 (1990).
2. **Rojas, G., Almagro, J. C., Acevedo, B., and Gavilondo, J. V.:** Phage antibody fragments library combining a single human light chain variable region with immune mouse heavy chain variable regions, J. Biotechnol., **94**, 287–298 (2002).
3. **Honjo, T. and Habu, S.:** Origin of immune diversity: genetic variation and selection, Annu. Rev. Biochem., **54**, 803–830 (1985).
4. **Adams, G. P. and Weiner, L. M.:** Monoclonal antibody therapy of cancer, Nat. Biotechnol., **23**, 1147–1157 (2005).
5. **Griffiths, A. D. and Duncan, A. R.:** Strategies for selection of antibodies by phage display, Curr. Opin. Biotechnol., **9**, 102–108 (1998).
6. **Nieri, P., Donadio, E., Rossi, S., Adinolfi, B., and Podesta, A.:** Antibodies for therapeutic uses and the evolution of biotechniques, Curr. Med. Chem., **16**, 753–779 (2009).
7. **Richter, S. N., Frasson, I., and Palu, G.:** Strategies for inhibiting function of HIV-1 accessory proteins: a necessary route to AIDS therapy, Curr. Med. Chem., **16**, 267–286 (2009).
8. **Fackler, O. T., Alcover, A., and Schwartz, O.:** Modulation of the immunological synapse: a key to HIV-1 pathogenesis, Nat. Rev. Immunol., **7**, 310–317 (2007).
9. **Imai, S., Mukai, Y., Nagano, K., Shibata, H., Sugita, T., Abe, Y., Nomura, T., Tsutsumi, Y., Kamada, H., Nakagawa, S., and Tsunoda, S.:** Quality enhancement of the non-immune phage scFv library to isolate effective antibodies, Biol. Pharm. Bull., **29**, 1325–1330 (2006).
10. **Lo, A. S., Zhu, Q., and Marasco, W. A.:** Intracellular antibodies (intrabodies) and their therapeutic potential, Handb. Exp. Pharmacol., **181**, 343–373 (2008).
11. **Worn, A., Auf der Maur, A., Escher, D., Honegger, A., Barberis, A., and Pluckthun, A.:** Correlation between in vitro stability and in vivo performance of anti-GCN4 intrabodies as cytoplasmic inhibitors, J. Biol. Chem., **275**, 2795–2803 (2000).

Provided for non-commercial research and education use.
Not for reproduction, distribution or commercial use.

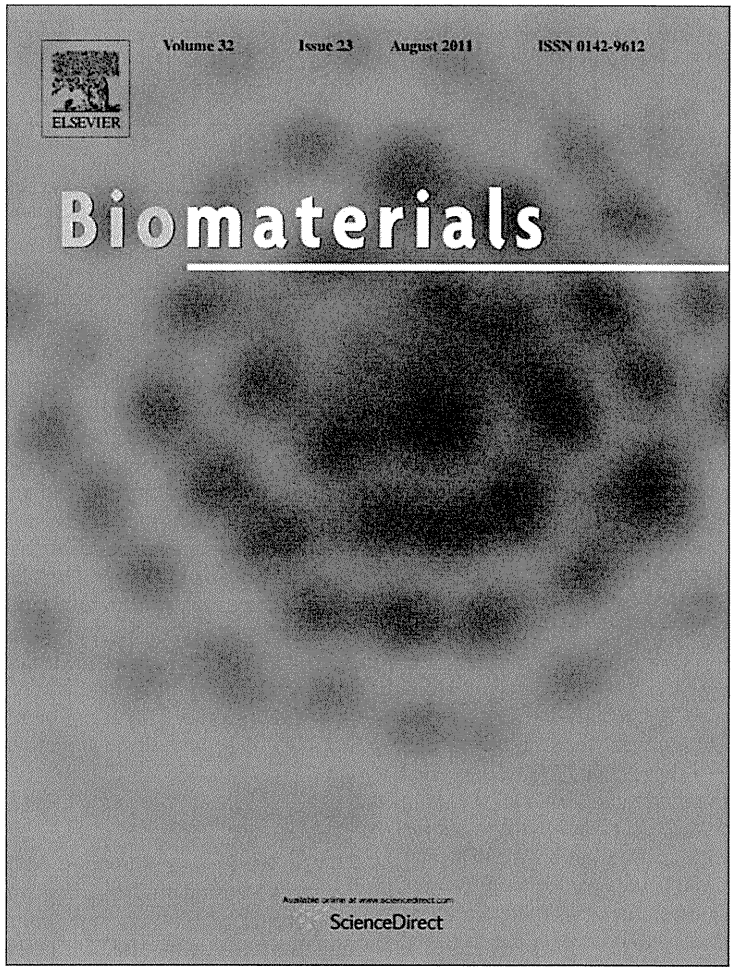

This article appeared in a journal published by Elsevier. The attached copy is furnished to the author for internal non-commercial research and education use, including for instruction at the authors institution and sharing with colleagues.

Other uses, including reproduction and distribution, or selling or licensing copies, or posting to personal, institutional or third party websites are prohibited.

In most cases authors are permitted to post their version of the article (e.g. in Word or Tex form) to their personal website or institutional repository. Authors requiring further information regarding Elsevier's archiving and manuscript policies are encouraged to visit:

http://www.elsevier.com/copyright

Author's personal copy

Biomaterials 32 (2011) 5498–5504

Contents lists available at ScienceDirect

Biomaterials

journal homepage: www.elsevier.com/locate/biomaterials

Fine tuning of receptor-selectivity for tumor necrosis factor-α using a phage display system with one-step competitive panning

Yasuhiro Abe [a], Tomoaki Yoshikawa [a,b], Masaki Inoue [a], Tetsuya Nomura [a], Takeshi Furuya [a,b], Takuya Yamashita [a,b], Kazuya Nagano [a], Hiromi Nabeshi [a,b], Yasuo Yoshioka [a,c], Yohei Mukai [a,b], Shinsaku Nakagawa [b,c], Haruhiko Kamada [a,c], Yasuo Tsutsumi [a,b,c], Shin-ichi Tsunoda [a,b,c,*]

[a] Laboratory of Biopharmaceutical Research, National Institute of Biomedical Innovation, 7-6-8 Saito-Asagi, Ibaraki, Osaka 567-0085, Japan
[b] Graduate School of Pharmaceutical Sciences, Osaka University, 1-6 Yamadaoka, Suita, Osaka 565-0871, Japan
[c] The Center of Advanced Medical Engineering and informatics, Osaka University, 1-6 Yamadaoka, Suita, Osaka 565-0871, Japan

ARTICLE INFO

Article history:
Received 24 March 2011
Accepted 5 April 2011
Available online 5 May 2011

Keywords:
Cytokine
Molecular biology
Protein
Affinity
Bioactivity

ABSTRACT

Tumor necrosis factor-α (TNF) is one of the attractive targets for the development of anti-inflammatory and anti-tumor drugs, because it is an important mediator in the pathogenesis of several inflammatory diseases and tumor progression. Thus, there is an increasing need to understand the TNF receptor (TNFR1 and TNFR2) biology for the development of TNFR-selective drugs. Nonetheless, the role of TNFRs, especially that of TNFR2, remains poorly understood. Here, using a unique competitive panning, we optimized our phage display-based screening technique for isolating receptor-selective TNF mutants, and identified several TNFR2-specific TNF mutants with high TNFR2 affinity and full bioactivity via TNFR2. Among these mutants, the R2-7 clone revealed very high TNFR2-selectivity (1.8×10^5 fold higher than that for the wild-type TNF), which is so far highest among the reported TNFR2-selective TNF mutants. Because of its high TNFR2-selectivity and full bioactivity, the TNF mutant R2-7 would not only help in elucidating the functional role of TNFR2 but would also help in understanding the structure-function relationship of TNF/TNFR2. In summary, our one-step competitive panning system is a simple, useful and effective technology for isolating receptor-selective mutant proteins.

© 2011 Elsevier Ltd. All rights reserved.

1. Introduction

Tumor necrosis factor-α (TNF) is a major inflammatory cytokine that plays a central role in host defense and inflammation via two receptor subtypes, TNF receptor (TNFR)1 and TNFR2 [1,2]. Elevated serum levels of TNF correlates with the severity and progression of the inflammatory diseases such as rheumatoid arthritis (RA), inflammatory bowel disease, septic shock, multiple sclerosis and hepatitis [3–5]. Currently, TNF-neutralization therapies have proven successful for the treatment of RA [4,6,7]. However, these therapies can cause serious side effects, such as tuberculosis, because TNF-dependent host defense functions are also inhibited [8,9]. Therefore, understanding the function of TNF/TNFRs is important for optimal therapy of various TNF-related autoimmune diseases. TNFR1 is constitutively expressed in most tissues and seems to be the key mediator of TNF signaling [10,11]. In contrast, the expression of TNFR2 is more restricted and is found mainly on certain T-cell subpopulations [12], endothelial cells, cardiac myocytes [13] and neuronal tissue [14,15]. Recent studies suggested that TNFR2 signaling is associated with T-cell survival [16], cardioprotection [17,18], remyelination [19], and survival of some neuron subtypes [20,21]. Although the two TNFRs have been shown to have distinct functions in some cells [22], the physiological significance of the presence of both receptors is not fully understood. Especially TNFR2-induced signaling remains elusive and need further investigation.

In order to understand the mechanism of TNFRs, we have investigated the relationship between the biological activities and structural properties of a large number of TNF mutants by phage-display technique [23,24]. However, screening efficiency of isolating TNFR2-selective TNF mutants using this technique is extremely low, and it is difficult to prepare large repertoire of TNFR2-selective TNF mutants for the structure-activity relationship study. In our previous study, we screened 500 phage clones

* Corresponding author. Laboratory of Biopharmaceutical Research, National Institute of Biomedical Innovation, 7-6-8 Saito-Asagi, Ibaraki, Osaka 567-0085, Japan. Tel.: +81 72 641 9814; fax: +81 72 6419817.
E-mail address: tsunoda@nibio.go.jp (S.-i. Tsunoda).

0142-9612/$ – see front matter © 2011 Elsevier Ltd. All rights reserved.
doi:10.1016/j.biomaterials.2011.04.018

Author's personal copy

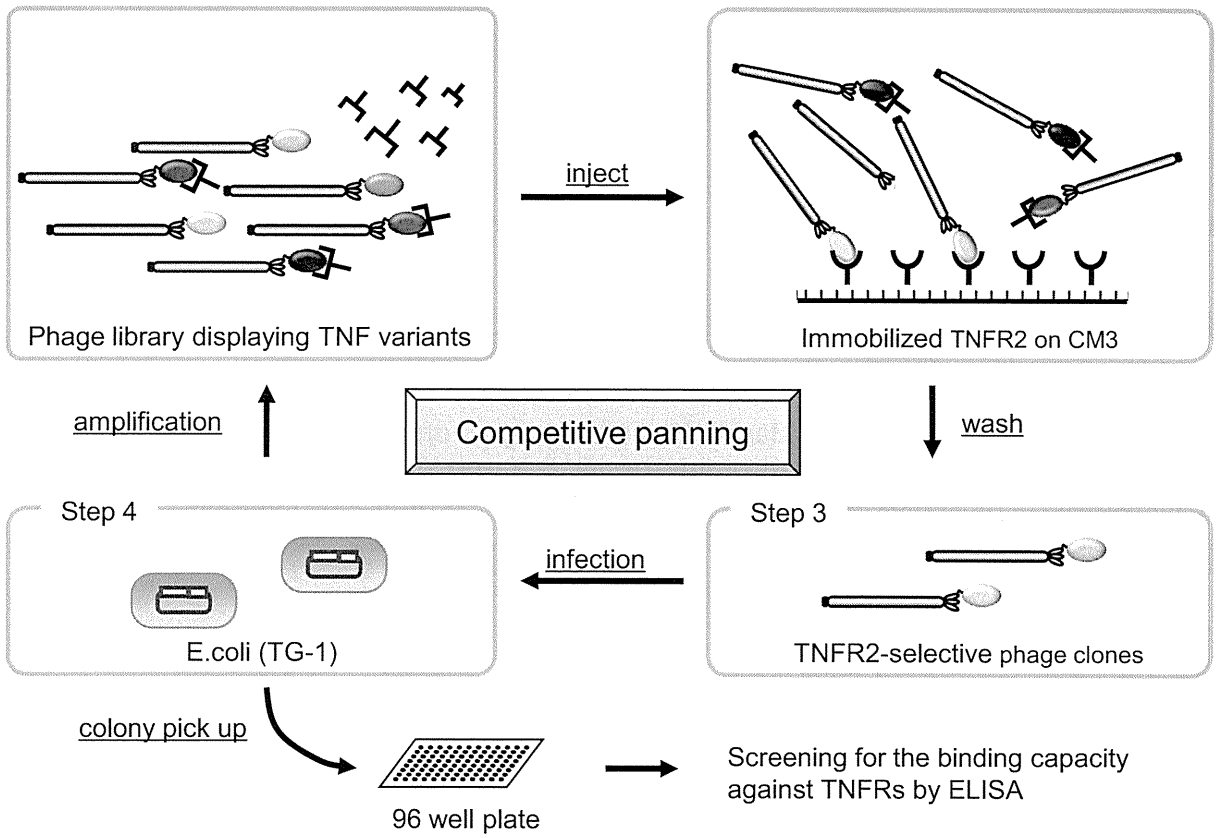

Fig. 1. Screening scheme for isolating TNFR2-selective TNF mutants using competitive panning. To concentrate TNFR2-selective mutant TNFs, phage libraries were pre-incubated with TNFR1 Fc chimera (TNFR1-Fc), and subsequent biopanning against the TNFR2 was carried out in the presence of TNFR1-Fc using the BIAcore biosensor. After several rounds of panning, phage clones were isolated and screened by ELISA.

for isolating TNFR2-selective mutants using the conventional panning method [23]. Out of the 500 clones, only 2 clones showed selectivity for TNFR2 binding that was 10-times higher than the wild-type TNF (wtTNF). Furthermore, bioactivities of these two TNFR2 selective TNF mutants were lower than that of wtTNF (<30%). To improve the screening efficacy, we optimized our phage display-based cytokine mutagenesis technology [25] with an unique competitive panning technique for identifying TNFR2-specific TNF mutants with higher affinity and bioactivity. In this competitive panning technique, phage libraries were pre-incubated with TNFR1 Fc chimera (TNFR1-Fc), and subsequent biopanning against the TNFR2 was carried out in the presence of TNFR1-Fc using the BIAcore biosensor. Since TNFR1-binding clones could not bind to TNFR2 due to steric hindrance, TNF mutants binding only to TNFR2 were selectively enriched with high efficiency. Using this optimized competitive panning technique, we have identified TNFR2-selective TNF mutants with full bioactivity via TNFR2.

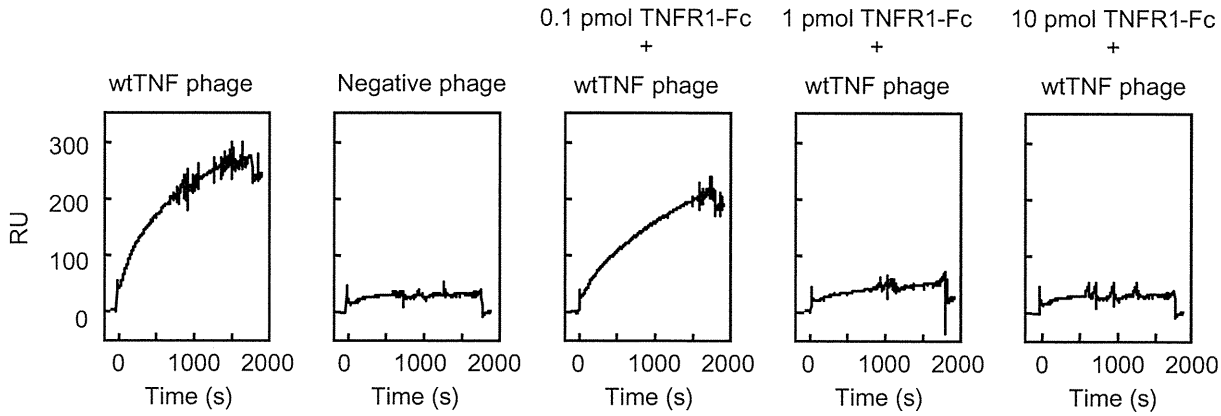

Fig. 2. Optimization of competitive panning using BIAcore biosensor. 0.1 pmol, 1 pmol or 10 pmol of human TNFR1-Fc was mixed with 1×10^{10} CFU phages displaying wtTNF for 2 h at 4 °C, and the mixture was passed over the TNFR2-immobilized CM3 sensor chip and real-time biomolecular interaction analyses were performed with BIAcore biosensor. Anti-CD25 single chain Fv-displaying phage was used as a negative control.

Author's personal copy

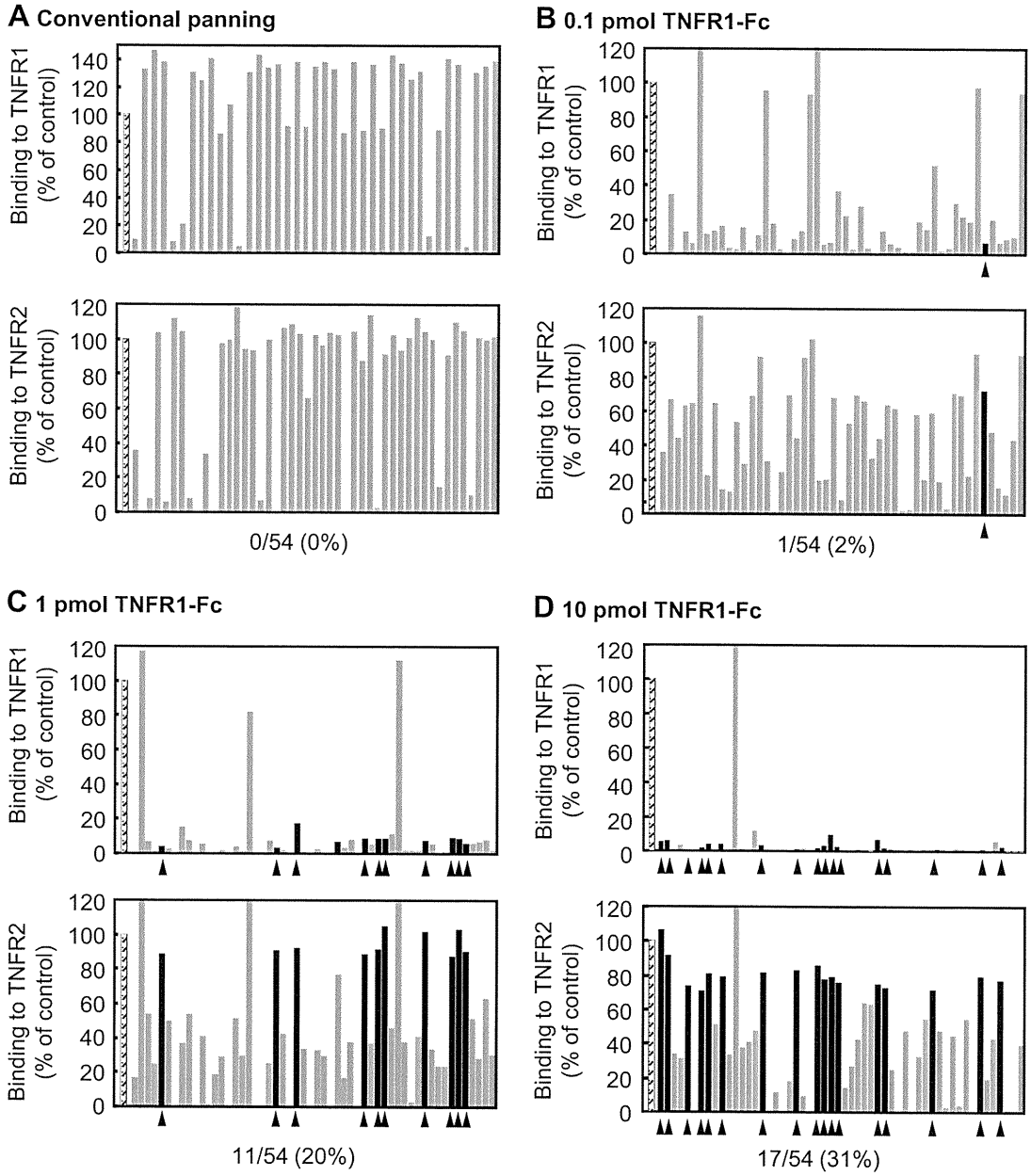

Fig. 3. Determination of relative affinities of mutant TNFs for TNFR1 or TNFR2 by capture ELISA. *E. coli* supernatant containing a TNF mutant (gray bar) from each panning conditions, in which phages were premixed with (A) none, (B) 0.1 pmol, (C) 1 pmol and (D) 10 pmol of TNFR1-Fc, were applied to the TNFR1-Fc or TNFR2-Fc immobilized plate and detected with biotinylated polyclonal anti-TNF antibody. wtTNF was used as a positive control (hatched bar). Affinities of TNFR2-selective clones (black bar) for TNFR2 was more than 70% of that of the wtTNF, and that for TNFR1 was less than 30% of that of the wtTNF.

2. Materials and methods

2.1. Cells

HEp-2 cells, a human fibroblast cell line, were provided by Cell Resource Center for Biomedical Research (Tohoku University, Sendai, Japan) and were maintained in RPMI 1640 (Sigma–Aldrich Japan, Tokyo, Japan) supplemented with 10% bovine fetal serum (FBS) 1 mM sodium pyruvate, 50 mM 2-mercaptoethanol, and antibiotics. hTNFR2/mFas-PA cells are preadipocytes derived from TNFR1$^{-/-}$R2$^{-/-}$ mice expressing a chimeric receptor, the extracellular and transmembrane domain of human TNFR2, and intracellular domain of mouse Fas; these cells were cultured in RPMI 1640 supplemented with 10% FBS, 5 μg/ml Blasticidin S HCl (Invitrogen, Carlsbad, CA), and antibiotics [26].

2.2. Library construction

Protocol for the construction of phage-display library displaying structural mutants of human TNF has been described previously [23]. In brief, multiple-mutations were introduced into the wtTNF gene by PCR to randomly replace the codons of 6 amino acid residues at positions 29, 31, 32, 145, 146 and 147, respectively, of the TNF protein. The PCR product was digested with the restriction enzymes Hind III and Not I, and ligated into the Hind III/Not I digested pY03′ phagemid vector for displaying the TNF mutants on the phage surface as g3p-fusion proteins.

2.3. Optimization of competitive panning using BIAcore biosensor

Human TNFR2-Fc (R&D systems, Minneapolis, MN) was diluted to 50 μg/ml in 10 mM sodium acetate buffer (pH 4.5) and immobilized onto a CM3 sensor chip using an amine coupling kit (GE Healthcare, UK), which resulted in an increase of 5000–6000 resonance units (RU). 0.1 pmol, 1 pmol or 10 pmol of human TNFR1-Fc (R&D systems) was mixed with 100 μl of wtTNF-displaying phage (1×10^{11} CFU/ml) for 2 h at 4 °C, and the mixture was passed over the TNFR2-immobilized CM3 sensor chip at a flow rate of 3 μl/min. The binding kinetics of the mixtures to TNFR2-Fc were analyzed by BIAcore 2000 (GE Healthcare).

Author's personal copy

Table 1
Amino acid sequences of wtTNF and TNFR2-selective TNF mutants.

Clone	Residue position					
	29	31	32	145	146	147
wtTNF	L	R	R	A	E	S
R2–6	L	R	R	H	E	D
R2–7	V	R	R	D	D	D
R2–8	L	R	R	N	D	D
R2–9	L	R	R	T	S	D
R2–10	L	R	R	Q	D	D
R2–11	L	R	R	T	D	D
R2–12	L	R	R	D	G	D
R2–13	L	R	R	D	E	D

2.4. Selection of phage displaying TNFR2-selective TNF mutants by competitive panning

1×10^{10} CFU phages displaying TNF mutants were pre-incubated for 2 h at 4 °C, with serially diluted TNFR1-Fc. The mixtures were injected at 3 μl/min over the sensor chip. After injection, the sensor chip was washed using the rinse command for 3 min. Elution was carried out using 20 μl of 10 mM glycine-HCl (pH 2.0) and the eluted phage was neutralized with 1 M Tris–HCl (pH 6.9). The recovered phages were amplified by infection of E. coli strain TG1 (Stratagene, La Jolla, CA), which allow read-through of the amber stop codon located between the TNF and g3p sequences of pY03′ phagemid vector. These steps were repeated twice. After final round of panning, the phage mixture was used to infect E. coli and plated on LB agar/ampicillin plates. Single clones of transfected TG1 were randomly picked from the plate and each colony was grown in 2-YT medium with ampicillin (100 μg/ml) and glucose (2% w/v) at 37 °C until the OD_{600} of the culture medium reached 0.4. Each culture was centrifuged, the supernatants were removed, and fresh 2-YT media with ampicillin (100 μg/ml) was added to each E. coli pellet. After incubation for 6 h at 37 °C supernatants were collected and used to determine affinity for TNFRs by capture ELISA as described previously [24]. After the procedure, the phagemid vectors were sequenced using a Big Dye Terminator v3.1 kit and ABI PRISM 3100 (Applied Biosystems Ltd., Pleasanton, CA).

2.5. Expression and purification of TNF mutants

Preparation of purified recombinant protein was described previously [25]. In brief, TNF mutants recombined into pYas1 vector, under the control of T7 promoter, were produced in E. coli (BL21λDE3). Mutant TNFs recovered from inclusion body, which were washed in Triton X-100 and solubilized in 6 M guanidine-HCl, 0.1 M Tris–HCl, pH 8.0, and 2 mM EDTA. Solubilized protein was adjusted to 10 mg/ml and was reduced with 10 mg/ml dithioerythritol for 4 h at RT and refolded by 100-fold dilution in a refolding buffer (100 mM Tris–HCl, 2 mM EDTA, 1 M arginine, and oxidized glutathione (551 mg/L)). After dialysis with 20 mM Tris–HCl, pH 7.4, containing 100 mM urea, active trimeric proteins were purified by Q-Sepharose (GE Healthcare)chromatography and size-exclusion chromatography (Superose 12; GE Healthcare).

2.6. Analysis of binding kinetics using surface plasmon resonance (SPR)

The binding kinetics of the wtTNF and TNF mutants were analyzed by the SPR technique (BIAcore 2000; GE Healthcare). TNFR1-Fc or TNFR2-Fc were separately immobilized on to CM5 sensor chip, resulting in an increase of 3000–3500 RU. During the association phase, wtTNF or TNF mutants diluted in running buffer (HBS-EP) at 156.8, 52.3, 17.4, 5.8 or 1.9 nM were passed over the immobilized TNFR2 for 2 min at a flow rate of 20 μl/min. During the dissociation phase, HBS-EP was run over the sensor chip for 1 min at a flow rate of 20 μl/min. The SPR measurements for TNFR1 were performed using much higher concentrations of TNF mutants (392.1, 130.7, 43.6, 14.5 or 4.8 nM). The data were analyzed globally with BIAevaluation 3.1 software (GE Healthcare) to apply a 1:1 Langmuir binding model. The obtained sensorgrams were fitted globally over the range of injected concentrations and simultaneously over the association and dissociation phages.

2.7. In vitro assessment of bioactivity via TNFR1 or TNFR2 with TNF mutants

HEp-2 cells were seeded at 4×10^4 cells/well in 96-well plates and incubated for 18 h with serially diluted wtTNF (Peprotech, Rocky Hill, NJ) or TNF mutants in the presence of 50 mg/ml cycloheximide. After incubation, cell survival was determined by methylene blue assay as described previously [25]. In the case of analyzing TNFR2-mediated biological activity, hTNFR2/mFas-PA were seeded on 96-well micro titer plates with a density of 1.5×10^4 cells/well in culture medium. Serial dilutions of wtTNF (Peprotech) and TNF mutants were prepared with 1 μg/ml cycloheximide and added to each well. After 48 h-incubation at 37 °C, the cell viabilities were analyzed using a WST-8 assay kit (Nacalai Tesque) according to the manufacturer's instructions.

3. Results

3.1. Optimization of one-step competitive panning protocol

To improve identifying TNFR2-selective TNF mutants with better bioactivity, we have introduced a step to remove the TNFR1-binding phages from the library by competitive panning using TNFR1-Fc. We postulated that TNFR1-binding clones could be eliminated when panning for the TNFR2-binding clones is performed in the presence of TNFR1 protein (see Fig. 1). Although an immunoplate or immunotube is commonly used for the panning [27–29], these techniques cannot make real-time observation of the interaction between phage library and receptor, and are difficult to automate and control the precise settings. Therefore, we first utilized the BIAcore biosensor and optimized the concentration of TNFR1-Fc required for eliminating the TNFR1-binding clones. Serially diluted human TNFR1-Fc was mixed with 1×10^{10} CFU phages displaying wtTNF, and the binding avidity of the phage-displayed wtTNF for TNFR2 was assessed using a BIAcore biosensor. As shown in Fig. 2, TNFR1-Fc inhibited the binding of phage-displayed wtTNF to TNFR2 in a dose-dependent manner. 10 pmol of TNFR1-Fc virtually abolished the binding of wtTNF not only to TNFR2 (last panel in Fig. 2) but also the binding of wtTNF to TNFR1 (data not shown). These results clearly suggest that 10 pmol of TNFR1-Fc would be sufficient for competitively subtract unwanted TNFR1-binding phage clones from a phage library displaying structural TNF mutants.

Table 2
Biding kinetics of TNFs to TNFR1 and TNFR2.

	TNFR1				TNFR2			
	k_{on}[a] (10^6 $M^{-1}s^{-1}$)	k_{off}[b] (10^{-4} s^{-1})	K_D[c] (10^{-10} M)	Relative[d] (%)	k_{on}[a] (10^6 $M^{-1}s^{-1}$)	k_{off}[b] (10^{-4} s^{-1})	K_D[c] (10^{-10} M)	Relative[d] (%)
wtTNF	0.45	1.3	2.9	100.0	2.0	12.1	6.1	100.0
R2–6	0.79	54.5	68.8	4.2	3.2	7.8	2.4	251.4
R2–7	0.44	116.0	262.0	1.1	2.1	7.4	3.6	169.7
R2–8	1.22	50.3	41.1	7.1	3.1	6.6	2.1	291.0
R2–9	1.19	50.1	42.3	6.9	3.8	12.6	3.3	185.2
R2–10	0.67	43.9	63.7	4.6	2.2	5.3	2.4	253.5
R2–11	0.81	87.5	108.	2.7	2.3	5.4	2.3	264.5
R2–12	1.36	98.8	72.6	4.0	4.1	10.6	2.6	235.0
R2–13	0.97	104.0	107.0	2.7	2.9	8.2	2.9	212.2

Kinetic parameters for each TNF were calculated from the respective sensorgram by BIAevaluation 3.1software, and taking into consideration that the TNF binds as a trimer.
[a] k_{on} is the association kinetic constant.
[b] k_{off} is the dissociation kinetic constant.
[c] K_D is the equilibrium dissociation constant ($K_D = k_{off}/k_{on}$).
[d] Relative values were calculated from the K_D (wtTNF)/K_D (TNF mutants) × 100.

Author's personal copy

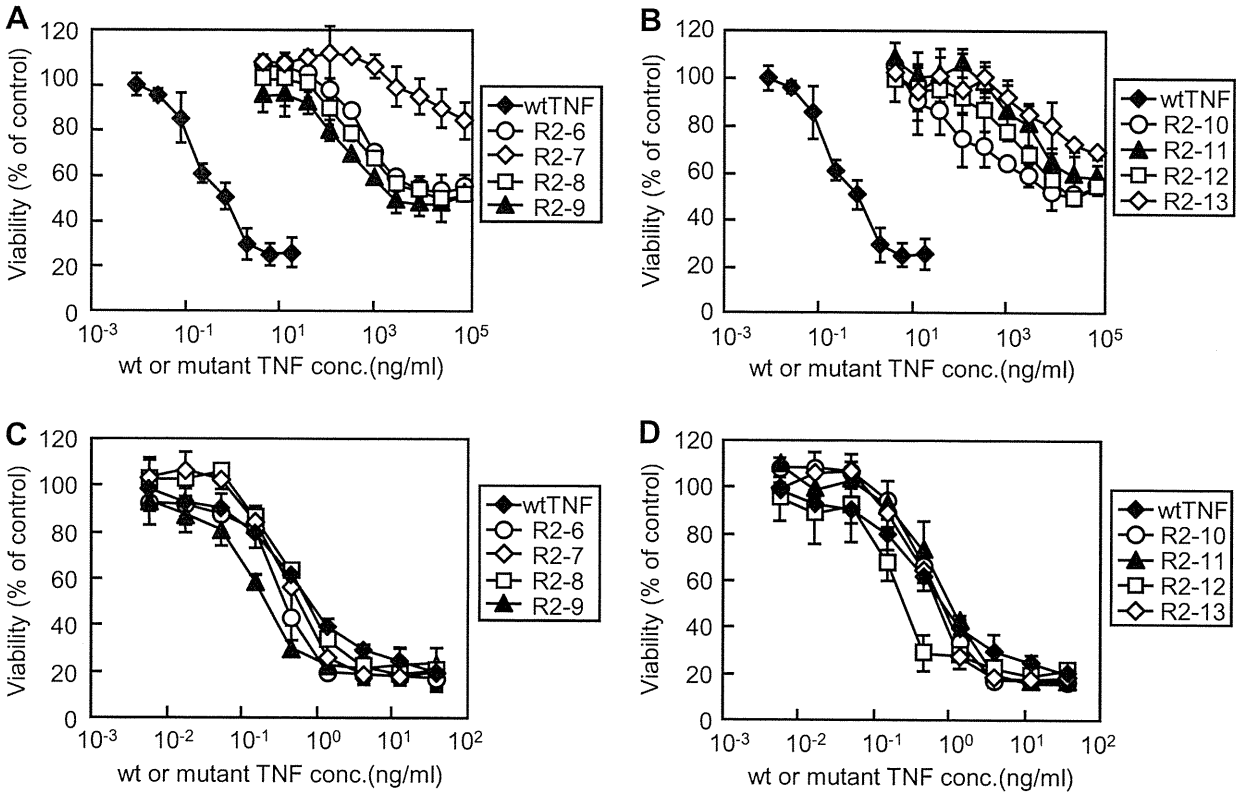

Fig. 4. In vitro bioactivity assay of TNF mutants via TNFR1 or TNFR2. The bioactivity of mutant TNFs via TNFR1 or TNFR2 were measured by cytotoxicity assay against HEp-2 cells (A and B) or hTNFR2/mFas-PA (C and D), respectively. Each point represents the mean ± S.D. of triplicate measurements.

3.2. Selection of TNFR2-selective TNF mutants by one-step competitive panning

To concentrate TNFR2-selective mutant TNFs, the TNF structural mutant displaying phage library was subjected to two rounds of conventional panning or competitive panning against TNFR2 using the BIAcore biosensor. After the second round of panning, *Escherichia coli* (TG1) supernatants of 54 randomly picked clones from each panning procedure were further screened by capture ELISA to analyze their binding specificities for each TNFR (Fig. 3). Consequently, we obtained numerous clones with high-affinity for TNFR2 under all panning conditions. Binding avidities of these clones for TNFR1 tended to decrease depending on the concentration of TNFR1-Fc used for premixing. However, binding avidity of a TNFR2-selective clone, which binds only to TNFR2 (Fig. 3, black bar), tended to increase depending on the concentration of TNFR1-Fc used for premixing. Almost all clones obtained from the conventional and competitive panning with 0.1 pmol of TNFR1-Fc (Fig. 3A and B, respectively) bound to TNFR1, and the panning efficiency for isolating the TNFR2-selective TNF mutants was <2%. In contrast, clones obtained from the subtracted panning with 1 or 10 pmol of TNFR1-Fc (Fig. 3C and D, respectively) contained many TNFR2-selective TNF mutants (>20%). From these panned clones, we eventually identified eight candidate agonists that selectively and strongly bound to the TNFR2. Amino acid sequences of these eight candidate TNFR2-selective TNF mutants are shown in Table 1. TNFR2-slective mutants were mutated near residue 145 and

Table 3
In vitro bioactivities of TNF mutants via TNFR1 or TNFR2.

	TNFR1[a]		TNFR2[b]		TNFR2/TNFR1[e]
	EC50[c] (ng/ml)	Relative Activity[d] (%)	EC50[c] (ng/ml)	Relative activity[d] (%)	
wtTNF	0.6	100	0.56	100	1.0
R2–6	8.1×10^{3}	7.3×10^{-3}	0.39	144	2.0×10^{4}
R2–7	$>1.0 \times 10^{5}$	$<6.0 \times 10^{-4}$	0.51	110	1.8×10^{5}
R2–8	4.6×10^{3}	1.2×10^{-2}	0.67	84	7.0×10^{3}
R2–9	2.1×10^{3}	2.8×10^{-2}	0.21	267	9.5×10^{3}
R2–10	1.1×10^{4}	5.4×10^{-3}	0.72	78	1.4×10^{4}
R2–11	6.7×10^{4}	8.9×10^{-4}	0.95	59	6.6×10^{4}
R2–12	2.6×10^{4}	2.2×10^{-3}	0.23	243	1.1×10^{5}
R2–13	$>1.0 \times 10^{5}$	$<6.0 \times 10^{-4}$	0.63	89	1.5×10^{5}

[a] Bioactivities of the wtTNF and TNF mutants via TNFR1 were measured by determining the TNF-induced cytotoxicity in HEp-2 cells.
[b] Bioactivities of the wtTNF and TNF mutants via TNFR2 were measured by determining the TNF-induced cytotoxicity in hTNFR2/mFas-PA.
[c] Experimental data were analyzed by a logistic regression model to calculate the mean effective concentration (EC50).
[d] Relative activities were calculated from the EC50 (wtTNF)/EC50 (TNF mutants).
[e] Selectivity for TNFR2 was calculated from the ratio of the relative activity (via TNFR2)/relative activity (via TNFR1).

Author's personal copy

conserved near residue 30. These findings indicate that the amino acid residues near position 30 are an essential for TNFR2 binding.

3.3. Binding kinetics of TNFR2-selective TNF mutants

To investigate the properties of eight TNFR2-selective TNF mutants in detail, we prepared recombinant protein using the previously described methods [30,31]. TNF mutants expressed as an inclusion body in *E. coli* (BL21λDE3) were denatured and refolded. Then, active TNF mutants were purified by ion–exchange and gel–filtration chromatography. TNF mutant purity was greater than 90% in sodium dodecyl sulfate–polyacrylamide gel electrophoresis, and all mutants were confirmed to form homotrimers in the same manner as the wtTNF by gel-filtration analysis (data not shown). To analyze the binding properties of these TNFR2-selective TNF mutants, we determined their binding dissociation constants (kinetic on- and off-rates) for TNFR1 and TNFR2, respectively, in detail using the surface plasmon resonance technique (Table 2). Our analysis showed that all eight mutant TNFs bound to the TNFR2 with high affinity; in contrast, they bound to the TNFR1 with greatly reduced affinity (typically between 1 and 7% of the wtTNF affinity). The dissociation constants (K_D) of these mutants for TNFR2 were between 2.1–3.6 $\times$ 10^{-10} M, and their relative affinities for TNFR2 were between 169 and 291% of that of the wtTNF. Thus, using the competitive panning technique we successfully obtained a large repertoire of TNFR2-selective TNF mutants with different binding parameters (on- and off-rates and dissociation constants).

3.4. Bioactivities of TNFR2-selective TNF mutants

To examine the bioactivity of these TNF mutants via TNFR1, we subsequently performed a cytotoxicity assay using HEp-2 cells (Fig. 4A and B). All TNF mutants (R2-6 ~ R2-13) showed almost no cytotoxicity, and the bioactivity was much lower than that of the wtTNF. Next, we evaluated the TNFR2-mediated activity of TNF mutants using the hTNFR2/mFas-PA, which were previously constructed in our laboratory [26]. The TNFR2-mediated bioactivities of these 8 mutant TNF proteins were at least same or higher than that of the wtTNF (Fig. 4C and D). As a negative control, we determined TNF cytotoxicity in parental TNFR1$^{-/-}$R2$^{-/-}$ preadipocytes and observed no wtTNF- or mutant TNF-mediated cell death (data not shown). Results of the cytotoxicity assay are summarized in Table 3. R2-7, the most highly TNFR2-selective mutant, exhibited 1.8 $\times$ 10^5 fold higher TNFR2-selectivity than that for the wild-type TNF.

4. Discussion

Recently, it was revealed that the two TNFRs worked together by crosstalk signaling, which suggested that the TNF-mediated signaling in the presence of both TNF receptors actually correlates with their physiological functions [32–34]. To understand the mechanism as well as to analyze the structure–function relationship of the TNFRs, several attempts were made in the past to create TNFR-specific mutant TNFs by conventional site-directed mutagenesis methods (such as Kunkel's method) [35–37]. However, these attempts were not very successful in yielding a desired TNF mutant having high receptor specificity and full bioactivity. For example, the TNFR2-binding affinity of the double mutant D143N-A145R was about 5–10 fold less than the wtTNF [38]. To overcome these problems, we applied phage-display technique and optimized panning method using the BIAcore biosensor (Fig. 1). Using an adequate amount of selective competitive inhibitor (>1 pmol TNFR1-Fc), this one-step competitive panning is ten times more efficient for screening TNFR2-selective TNF mutants, suggesting the competitive panning technology described here is a simple and effective screening method for fine-tuning TNF receptor-selectivity (Fig. 3). As a result of screening, we obtained successfully obtained TNFR2-selective TNF mutants with full bioactivity via TNFR2 (Table 3). Because of its high TNFR2-selectivity and full bioactivity, the TNF mutant R2-7 would help in elucidating the functional role of TNFR2.

One advantage of our phage-display-based technique is that it can be used to obtain the sequence information of many mutants [39,40]. It was previously shown by site-specific mutagenesis technique that mutations at positions 29, 31 and 32 (L29S, R31E and R32W) remarkably reduced the TNF's affinity for binding to TNFR2 [35,37,38]. For most of the TNFR2-selective TNF mutants, amino acids at positions 29, 31 and 32 were indeed identical (except for the R2-7 mutant which contained a conserved L to V substitution at position 29) to those of the wtTNF (Table 1), which is consistent with the previously reported idea that these three amino acids play critical roles in maintaining the binding between the TNF and TNFR2. The amino acid sequence at positions 145, 146 and 147 of the TNFR2-selective TNF mutants were, however, very different from those of the wtTNF. For example, the amino acid residue at position 145 of the TNF mutants R2-7, R2-12 and R2-13 contained an Asp residue in place of the Ala residue, and all of them showed high TNFR2 selectivity. Structural analysis and mutagenesis studies suggested that the loop containing the residues 145–147 is involved in the receptor binding [41–43]. Since Asp is a comparatively large residue, we speculated that this substitution could lead to a steric hindrance disrupting the interaction between the TNFR1 and TNFR2-selective mutants, which may be why they are less TNFR1-selective. However, why this replacement would increase the selectivity for TNFR2 is unclear at this moment. Currently, we are working on determining the structure of the TNF/TNFR2 complex by X-ray crystallography [44] so that structure–activity relationship studies could be initiated in the near future. Additionally, this structural information, in combination with bioinformatics technology, will be useful for designing TNFR-selective inhibitors (peptide mimics and chemical compounds).

5. Conclusions

In this study, we optimized our phage display-based screening using a unique competitive panning technique, which is ten times more efficient for screening TNFR2-selective TNF mutants compared to the conventional panning method. As a result of screening, we have succeeded in isolating several TNFR2-specific TNF mutants with high TNFR2 affinity and full bioactivity via TNFR2. Further analysis of the relationship between the structure and bioactivity of the TNF mutants would offer highly valuable and useful information regarding the TNF/TNFR biology. In conclusion, our fine-tuned competitive panning system is a simple and effective technology for isolating receptor-selective mutant proteins.

Acknowledgment

This study was supported in part by Grants-in-Aid for Scientific Research from the Ministry of Education, Culture, Sports, Science and Technology of Japan, and from the Japan Society for the Promotion of Science (JSPS). This study was also supported in part by Health Labour Sciences Research Grants from the Ministry of Health, Labor and Welfare of Japan, and by Health Sciences Research Grants for Research on Publicly Essential Drugs and Medical Devices from the Japan Health Sciences Foundation.

References

[1] Aggarwal BB. Signalling pathways of the TNF superfamily: a double-edged sword. Nat Rev Immunol 2003;3(9):745–56.
[2] Szlosarek PW, Balkwill FR. Tumour necrosis factor alpha: a potential target for the therapy of solid tumours. Lancet Oncol 2003;4(9):565–73.

Author's personal copy

[3] Aderka D, Engelmann H, Maor Y, Brakebusch C, Wallach D. Stabilization of the bioactivity of tumor necrosis factor by its soluble receptors. J Exp Med 1992; 175(2):323–9.
[4] Feldmann M, Maini RN. Lasker Clinical Medical Research Award. TNF defined as a therapeutic target for rheumatoid arthritis and other autoimmune diseases. Nat Med 2003;9(10):1245–50.
[5] Muto Y, Nouri-Aria KT, Meager A, Alexander GJ, Eddleston AL, Williams R. Enhanced tumour necrosis factor and interleukin-1 in fulminant hepatic failure. Lancet 1988;2(8602):72–4.
[6] Thorbecke GJ, Shah R, Leu CH, Kuruvilla AP, Hardison AM, Palladino MA. Involvement of endogenous tumor necrosis factor alpha and transforming growth factor beta during induction of collagen type II arthritis in mice. Proc Natl Acad Sci U S A 1992;89(16):7375–9.
[7] Williams RO, Feldmann M, Maini RN. Anti-tumor necrosis factor ameliorates joint disease in murine collagen-induced arthritis. Proc Natl Acad Sci U S A 1992;89(20):9784–8.
[8] Gomez-Reino JJ, Carmona L, Valverde VR, Mola EM, Montero MD. Treatment of rheumatoid arthritis with tumor necrosis factor inhibitors may predispose to significant increase in tuberculosis risk: a multicenter active-surveillance report. Arthritis Rheum 2003;48(8):2122–7.
[9] Lubel JS, Testro AG, Angus PW. Hepatitis B virus reactivation following immunosuppressive therapy: guidelines for prevention and management. Intern Med J 2007;37(10):705–12.
[10] Leist M, Gantner F, Jilg S, Wendel A. Activation of the 55 kDa TNF receptor is necessary and sufficient for TNF-induced liver failure, hepatocyte apoptosis, and nitrite release. J Immunol 1995;154(3):1307–16.
[11] Mori L, Iselin S, De Libero G, Lesslauer W. Attenuation of collagen-induced arthritis in 55-kDa TNF receptor type 1 (TNFR1)-IgG1-treated and TNFR1-deficient mice. J Immunol 1996;157(7):3178–82.
[12] Ware CF, Crowe PD, Vanarsdale TL, Andrews JL, Grayson MH, Jerzy R, et al. Tumor necrosis factor (TNF) receptor expression in T lymphocytes. Differential regulation of the type I TNF receptor during activation of resting and effector T cells. J Immunol 1991;147(12):4229–38.
[13] Irwin MW, Mak S, Mann DL, Qu R, Penninger JM, Yan A, et al. Tissue expression and immunolocalization of tumor necrosis factor-alpha in post-infarction dysfunctional myocardium. Circulation 1999;99(11):1492–8.
[14] Dopp JM, Sarafian TA, Spinella FM, Kahn MA, Shau H, de Vellis J. Expression of the p75 TNF receptor is linked to TNF-induced NFkappaB translocation and oxyradical neutralization in glial cells. Neurochem Res 2002;27(11):1535–42.
[15] Yang L, Lindholm K, Konishi Y, Li R, Shen Y. Target depletion of distinct tumor necrosis factor receptor subtypes reveals hippocampal neuron death and survival through different signal transduction pathways. J Neurosci 2002; 22(8):3025–32.
[16] Ban L, Zhang J, Wang L, Kuhtreiber W, Burger D, Faustman DL. Selective death of autoreactive T cells in human diabetes by TNF or TNF receptor 2 agonism. Proc Natl Acad Sci U S A 2008;105(36):13644–9.
[17] Monden Y, Kubota T, Inoue T, Tsutsumi T, Kawano S, Ide T, et al. Tumor necrosis factor-alpha is toxic via receptor 1 and protective via receptor 2 in a murine model of myocardial infarction. Am J Physiol Heart Circ Physiol 2007;293(1):H743–53.
[18] Wang M, Crisostomo PR, Markel TA, Wang Y, Meldrum DR. Mechanisms of sex differences in TNFR2-mediated cardioprotection. Circulation 2008;118(Suppl. 14):S38–45.
[19] Arnett HA, Mason J, Marino M, Suzuki K, Matsushima GK, Ting JP. TNF alpha promotes proliferation of oligodendrocyte progenitors and remyelination. Nat Neurosci 2001;4(11):1116–22.
[20] Faustman D, Davis M. TNF receptor 2 p.thway: drug target for autoimmune diseases. Nat Rev Drug Discov 2010;9(6):482–93.
[21] Fontaine V, Mohand-Said S, Hanoteau N, Fuchs C, Pfizenmaier K, Eisel U. Neurodegenerative and neuroprotective effects of tumor Necrosis factor (TNF) in retinal ischemia: opposite roles of TNF receptor 1 and TNF receptor 2. J Neurosci 2002;22(7). RC216.
[22] MacEwan DJ. TNF receptor subtype signalling: differences and cellular consequences. Cell Signal 2002;14(6):477–92.
[23] Mukai Y, Shibata H, Nakamura T, Yoshioka Y, Abe Y, Nomura T, et al. Structure-function relationship of tumor necrosis factor (TNF) and its receptor interaction based on 3D structural analysis of a fully active TNFR1-selective TNF mutant. J Mol Biol 2009;385(4):1221–9.
[24] Shibata H, Yoshioka Y, Ohkawa A, Minowa K, Mukai Y, Abe Y, et al. Creation and X-ray structure analysis of the tumor necrosis factor receptor-1-selective mutant of a tumor necrosis factor-alpha antagonist. J Biol Chem 2008;283(2):998–1007.
[25] Yamamoto Y, Tsutsumi Y, Yoshioka Y, Nishibata T, Kobayashi K, Okamoto T, et al. Site-specific PEGylation of a lysine-deficient TNF-alpha with full bioactivity. Nat Biotechnol 2003;21(5):546–52.
[26] Abe Y, Yoshikawa T, Kamada H, Shibata H, Nomura T, Minowa K, et al. Simple and highly sensitive assay system for TNFR2-mediated soluble- and transmembrane-TNF activity. J Immunol Methods 2008;335(1–2):71–8.
[27] Schwarz M, Rottgen P, Takada Y, Le Gall F, Knackmuss S, Bassler N, et al. Single-chain antibodies for the conformation-specific blockade of activated platelet integrin alphaIIbbeta3 designed by subtractive selection from naive human phage libraries. Faseb J 2004;18(14):1704–6.
[28] Popkov M, Rader C, Barbas 3rd CF. Isolation of human prostate cancer cell reactive antibodies using phage display technology. J Immunol Methods 2004; 291(1–2):137–51.
[29] Eisenhardt SU, Schwarz M, Bassler N, Peter K. Subtractive single-chain antibody (scFv) phage-display: tailoring phage-display for high specificity against function-specific conformations of cell membrane molecules. Nat Protoc 2007;2(12):3063–73.
[30] Shibata H, Yoshioka Y, Abe Y, Ohkawa A, Nomura T, Minowa K, et al. The treatment of established murine collagen-induced arthritis with a TNFR1-selective antagonistic mutant TNF. Biomaterials 2009;30(34):6638–47.
[31] Shibata H, Yoshioka Y, Ikemizu S, Kobayashi K, Yamamoto Y, Mukai Y, et al. Functionalization of tumor necrosis factor-alpha using phage display technique and PEGylation improves its antitumor therapeutic window. Clin Cancer Res 2004;10(24):8293–300.
[32] Wajant H, Pfizenmaier K, Scheurich P. Tumor necrosis factor signaling. Cell Death Differ 2003;10(1):45–65.
[33] Weiss T, Grell M, Siemienski K, Muhlenbeck F, Durkop H, Pfizenmaier K, et al. TNFR80-dependent enhancement of TNFR60-induced cell death is mediated by TNFR-associated factor 2 and is specific for TNFR60. J Immunol 1998; 161(6):3136–42.
[34] Fotin-Mleczek M, Henkler F, Samel D, Reichwein M, Hausser A, Parmryd I, et al. Apoptotic crosstalk of TNF receptors: TNF-R2-induces depletion of TRAF2 and IAP proteins and accelerates TNF-R1-dependent activation of caspase-8. J Cell Sci 2002;115(Pt. 13):2757–70.
[35] Yamagishi J, Kawashima H, Matsuo N, Ohue M, Yamayoshi M, Fukui T, et al. Mutational analysis of structure–activity relationships in human tumor necrosis factor-alpha. Protein Eng 1990;3(8):713–9.
[36] Barbara JA, Smith WB, Gamble JR, Van Ostade X, Vandenabeele P, Tavernier J, et al. Dissociation of TNF-alpha cytotoxic and proinflammatory activities by p55 receptor- and p75 receptor-selective TNF-alpha mutants. Embo J 1994; 13(4):843–50.
[37] Van Ostade X, Vandenabeele P, Everaerdt B, Loetscher H, Gentz R, Brockhaus M, et al. Human TNF mutants with selective activity on the p55 receptor. Nature 1993;361(6409):266–9.
[38] Loetscher H, Stueber D, Banner D, Mackay F, Lesslauer W. Human tumor necrosis factor alpha (TNF alpha) mutants with exclusive specificity for the 55-kDa or 75-kDa TNF receptors. J Biol Chem 1993;268(35):26350–7.
[39] Abe Y, Nomura T, Yoshioka Y, Kamada H, Tsunoda S, Tsutsumi Y. Anti-inflammatory effects of a Novel TNFR1-selective antagonistic TNF mutant on established murine collagen-induced arthritis. Adv Exp Med Biol 2011;691:493–500.
[40] Yoshioka Y, Watanabe H, Morishige T, Yao X, Ikemizu S, Nagao C, et al. Creation of lysine-deficient mutant lymphotoxin-alpha with receptor selectivity by using a phage display system. Biomaterials 2010;31(7):1935–43.
[41] Eck MJ, Sprang SR. The structure of tumor necrosis factor-alpha at 2.6 A resolution. Implications for receptor binding. J Biol Chem 1989;264(29):17595–605.
[42] Van Ostade X, Tavernier J, Fiers W. Structure–activity studies of human tumour necrosis factors. Protein Eng 1994;7(1):5–22.
[43] Idriss HT, Naismith JH. TNF alpha and the TNF receptor superfamily: structure-function relationship(s). Microsc Res Tech 2000;50(3):184–95.
[44] Mukai Y, Nakamura T, Yoshikawa M, Yoshioka Y, Tsunoda S, Nakagawa S, et al. Solution of the structure of the TNF-TNFR2 complex. Sci Signal 2010;3(148). ra83.